The Astrophysical Journal, 709:1157–1173, 2010 February 1 doi:10.1088/0004-637X/709/2/1157

ISOTOPIC ANALYSIS OF SUPERNOVA SiC AND Si_3N_4 GRAINS FROM THE QINGZHEN (EH3) CHONDRITE

Yangting Lin[1], Frank Gyngard[2], and Ernst Zinner[2]
[1] Key Laboratory of the Earth's Deep Interior, Institute of Geology and Geophysics, Chinese Academy of Sciences, Beijing 100029, China
[2] Laboratory for Space Sciences and the Physics Department, Washington University, St. Louis, MO 63130, USA
Received 2009 August 27; accepted 2009 December 9; published 2010 January 12

ABSTRACT

We report Al–Mg, Ca, and Ti isotopic data in 16 silicon carbide grains and four silicon nitride grains from the Qingzhen enstatite chondrite. Previous C, N, and Si isotopic measurements had identified these grains as type X grains, believed to have an origin in Type II supernovae (SNe). The grains analyzed include both subtypes X1 and X2. Twelve SiC and three Si_3N_4 grains show evidence for initial ^{26}Al, and eight SiC grains evidence for ^{44}Ti; 11 SiC grains have ^{49}Ti excesses, possibly indicating the initial presence of ^{49}V. A correlation with subtype is shown for ^{44}Ti: X2 grains that have the highest inferred ^{44}Ti/^{48}Ti ratios. A weaker correlation exists for N ratios: X2 grains with ^{12}C/^{13}C > 300 have higher ^{14}N/^{15}N ratios than X1 grains. We compare our data and data from previous reports with the SN models by Rauscher et al. The SN models can explain the C and N isotopic ratios fairly well if material from the ^{15}N-rich spike in the He/N zone of the 25 $M_\odot$ SN model is used. They also can explain the ^{44}Ti/^{48}Ti ratios of the X1 and X2 grains. For the latter, substantial contributions from the inner Ni core are required. They indicate that not for all grains the ^{49}Ti excesses can be attributed to decay of ^{49}V and material from the He/C zone, where ^{49}Ti is produced by neutron capture, is needed. The SN models, however, fail in explaining the Si isotopic ratios of most of the grains in a satisfactory fashion and the distinction between X1 and X2 grains. They also fail in explaining the observed correlation between the ^{26}Al/^{27}Al ratios and ^{12}C/^{13}C (and ^{14}N/^{15}N) ratios.

Key words: dust, extinction – nuclear reactions, nucleosynthesis, abundances – supernovae: general

Online-only material: color figure

1. INTRODUCTION

Primitive meteorites, interplanetary dust particles, and cometary dust contain tiny grains of stardust. These grains, also called presolar grains, are recognized as stardust on the basis of their anomalous isotopic compositions, and can be identified, isolated, and analyzed in detail in the laboratory (Clayton & Nittler 2004; Hoppe 2004; Lodders & Amari 2005; Lugaro 2005; Zinner 2007). Their isotopic ratios indicate that they condensed in expanding atmospheres of evolved stars and in ejecta from supernovae (SNe). Isotopic and microstructural studies of the grains provide a wealth of information on stellar nucleosynthesis, stellar evolution, Galactic chemical evolution, physical properties of stellar atmospheres, mixing of SN ejecta, interstellar dust processing, and conditions in the early Solar system. Presolar grains comprise carbonaceous phases (diamond, silicon carbide, and graphite), oxide phases (corundum, spinel, hibonite), and silicates.

Among all types of stardust, silicon carbide has been studied in most detail (e. g., Zinner 2007). According to their C and Si (and also N and Al) isotopic compositions, SiC grains have been classified into subtypes. Making up one of the rare subtypes are so-called X grains, which comprise only ∼1% of presolar SiC from the Murchison carbonaceous meteorite (Amari et al. 1992; Hoppe et al. 1996; Nittler et al. 1995). These grains are characterized by mostly ^{12}C, ^{15}N, and ^{28}Si enrichments, and high inferred ^{26}Al/^{27}Al ratios (up to 0.6). These isotopic signatures already indicated an origin in Type II SNe, since only SNe produce Si isotopic compositions with large ^{28}Si excesses (e.g., Woosley & Weaver 1995; Rauscher et al. 2002). The smoking gun for a SNII origin came from large ^{44}Ca excesses observed in a subset of X grains that must come from the decay of ^{44}Ti ($T_{1/2}$ = 60 yr) (Amari et al. 1992; Hoppe et al. 1996, 2000; Nittler et al. 1996; Besmehn & Hoppe 2003). Inferred ^{44}Ti/^{48}Ti ratios range up to 0.6. Titanium-44 is only produced in SNe; in Type II SNe it is synthesized in the Ni- and Si-rich inner zones (Woosley & Weaver 1995; Timmes et al. 1996). Many X grains also exhibit large ^{49}Ti excesses (Amari et al. 1992; Nittler et al. 1996), and Hoppe & Besmehn (2002) argued that they are due to decay of ^{49}V ($T_{1/2}$ = 336 d). In Type II SNe, ^{49}V is produced in the same layers as ^{44}Ti.

Although SiC of type X is rare, it can be preferentially located by ion imaging (Hoppe et al. 1996; Nittler et al. 1997; Lin et al. 2002; Besmehn & Hoppe 2003) or automatic isotopic measurements (Nittler & Alexander 2003) in the ion microprobe and subsequently analyzed in detail for the isotopic compositions of many elements. To date, more than 500 X grains have been identified.

Our previous analyses of SiC-X from the Qingzhen (EH3) meteorite have shown a bimodal pattern in their δ^{29}Si/δ^{30}Si values, with two peaks at 0.65 and 1.25, respectively (Lin et al. 2002). Delta-values are isotopic ratios expressed as permil (‰) deviations from the solar (terrestrial) ratios:

$$\delta^{29,30}\mathrm{Si}/^{28}\mathrm{Si} = 1000 \times ((^{29,30}\mathrm{Si}/^{28}\mathrm{Si})/(^{29,30}\mathrm{Si}/^{28}\mathrm{Si})_{\mathrm{solar}} - 1).$$

While most of the X grains in that study fall into the first group, about 25% of a total 36 grains are more depleted in ^{29}Si relative to ^{30}Si. These more ^{29}Si-deficient grains were referred to as X2 grains, in order to distinguish them from the more abundant X1 grains. This bimodal pattern is also seen among X grains from other meteorites. Figure 1 is a three-isotope δ-value plot of all X grains for which data are presently available (http://presolar.wustl.edu/∼pgd/). We define the grains that plot in the narrow band between the two lines as X1 grains, the grains plotting above as X0, and those plotting below as X2. Figure 2 shows a plot of the different types of X grains according to our definition. The correlation line for the type X1 grains has a slope

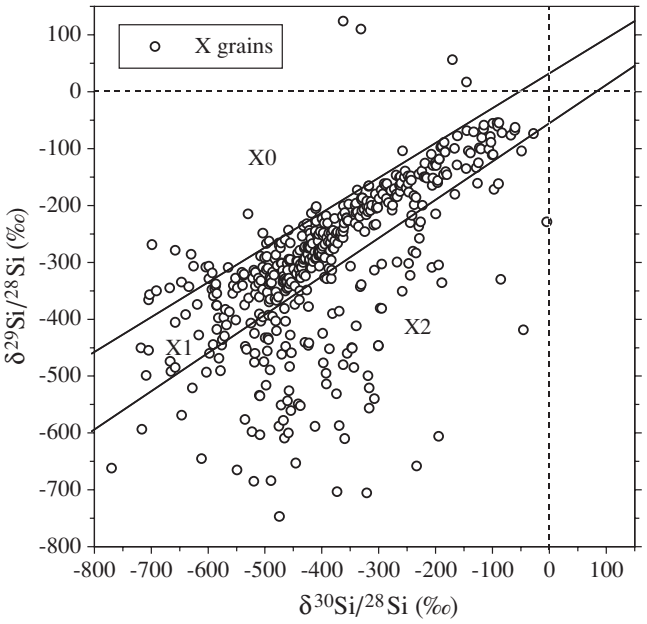

Figure 1. Silicon isotopic ratios of SiC grains of type X. The ratios are expressed as δ values, deviations from the solar (normal) ratios (broken lines) in permil (‰). Most grains lie between the two solid lines. They are defined as X1 grains and are distinguished from X0 grains, plotting above, and X2 grains, plotting below that region. The grain data are from the Presolar Database at http://presolar.wustl.edu/~pgd/.

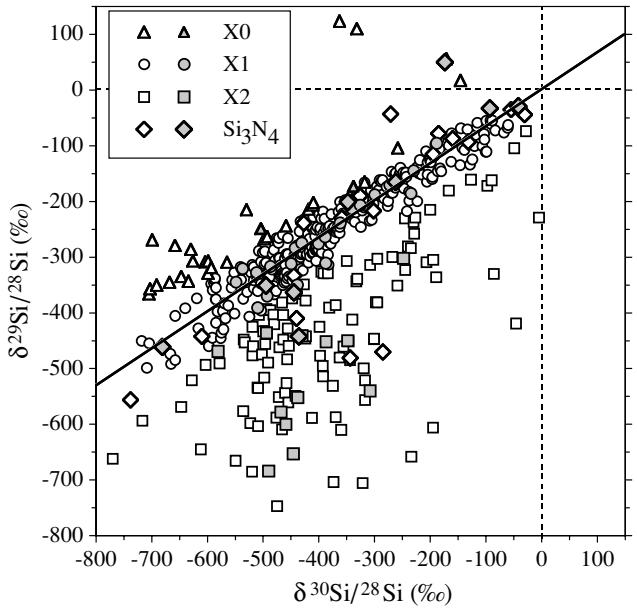

Figure 2. Silicon isotope ratio plot of subtypes of type X SiC grains. Also plotted are silicon nitride grains. In this and subsequent figures, the filled-in symbols are data from this study, the open symbols are data from other publications (http://presolar.wustl.edu/~pgd/). The solid line is a fit through the X1 grain data points.

of 0.66. Silicon nitride grains have ^{28}Si enrichments like SiC X grains and are also plotted.

In the Lin et al. (2002) study, we noticed already some correlation between the Si and C isotopic ratios of X grains: the ^{12}C/^{13}C ratios of the nine X2 grains are on average higher than those of the 27 X1 grains. During that study we identified 9 X type Si_3N_4 grains. In their C and Si isotopic compositions they appear to be closer to X1 than X2 grains.

In order to explore in more detail the differences between the X1 and X2 subtypes and to see whether these differences extend to the isotopic ratios of other elements, we measured isotopic and elemental compositions of Mg, Al, Ca, Ti, and V in the X grains from the Qingzhen enstatite meteorite previously identified (Lin et al. 2002). With these data we determine the inferred isotopic ratios of the short-lived nuclides ^{26}Al, ^{44}Ti, and possibly ^{49}V. The results are then compared with theoretical models of Type II SNe (Rauscher et al. 2002).

2. SAMPLES AND EXPERIMENTS

In our previous study (Lin et al. 2002), two size fractions, QZR4 (0.4–0.8 μm) and QZR5 (0.8–2 μm), of acid residues from Qingzhen were mapped for $^{16}O^-/^{18}O^-$ and $^{28}Si^-/^{30}Si^-$ ratios in the Cameca IMS 3f ion microprobe at Washington University. High-mass-resolution analyses of C, N, and Si were conducted on the ^{30}Si deficient Si-rich grains and led to the identification of 36 SiC X grains and nine type X Si_3N_4 grains. A total of 23 of the X grains (10 SiC-X1, 8 SiC-X2, 5 Si_3N_4) from the QZR4 and one of the QZR5 fractions were selected for the present study.

All of the X grains were re-located and examined in a JEOL 840A scanning electron microscope (SEM) equipped with an energy dispersive X-ray spectrometer (EDS). Significant X-ray signals of Al were detected in almost all X grains, while Mg was found in a smaller number of grains. The high-mass-resolution analyses of Al, Mg, Ca, Ti, and V isotopes were carried out with the CAMECA NanoSIMS 50 at Washington University. In order to avoid interference of Mg and Al from neighboring spinel ($MgAl_2O_4$) grains, only 15 of the X grains (12 SiC, 3 Si_3N_4), well separated from spinel, were analyzed for Mg isotopes and Al. Magnesium-24, ^{25}Mg, ^{26}Mg, ^{27}Al, and ^{28}Si were measured in multidetection by rastering a primary O^- beam of $\sim$10 pA over an area of 3 $\times$ 3 μm^2. Possible interferences from surroundings were avoided by accepting counts only from an area containing the grain within the raster area. After the Al–Mg measurements, the remaining grains (ten SiC-X, two Si_3N_4) and another six SiC-X grains and two Si_3N_4 grains were analyzed for Ca and Ti. Measurements were made in a combined mode of magnetic peak jumping and multidetection. During the first field step we detected ^{28}Si, ^{40}Ca, ^{44}Ca, ^{46}Ti, and ^{48}Ti, during the second field step ^{47}Ti, ^{49}Ti, and ^{51}V. Terrestrial spinel was used as a standard for Mg and Al, and perovskite ($CaTiO_3$) for the isotopes of Ca and Ti. For the determination of the elemental abundances of Ca, Ti, and V we used NIST Silicate Glass Certified Reference Material SRM 610 (previously NBS 610 glass; Kane 1998) as a standard.

As sensitivity factors of Mg and Al relative to Si we used the values 5.82 and 4.45 determined by Hoppe et al. (2000). The resulting Mg/Al sensitivity factor of 1.31 is not very different from the ratio of 1.25 we obtained from the terrestrial spinel standard. The sensitivity factors of Ca, Ti, and V relative to Si measured on SRM 610 are 10.8, 3.82, and 3.76, respectively. Except for Ti, they are quite similar to the ratios of 9.96, 4.57, and 3.89 of Hinton (1990) we obtain if we use the recently determined concentrations of 460 ppm and 462 ppm for Ti and V (Rocholl et al. 1997) instead of the values of 437 ppm and 500 ppm used by Hinton. Besmehn & Hoppe (2003) obtained 8.2 and 4.2 for the Ca/Si and Ti/Si sensitivity factors. Elemental sensitivity factors depend not only on the instrument but also on instrumental settings. We therefore use the values obtained by our measurements on SRM 610. Sensitivity factors also depend on the matrix. Our Ca/Ti factor of 2.83 is very different from the factor of 5.48 we obtain from perovskite, which in turn agrees

with the value of 5.6 measured by Hoppe et al. (2000). We think that the Ca/Ti sensitivity factor in SiC is probably closer to that in a silicate glass than in perovskite.

Radiogenic excesses of ^{26}Mg and ^{44}Ca (^{26}Mg* and ^{44}Ca*) were calculated by subtracting the "normal" components obtained by multiplying the ^{24}Mg and ^{40}Ca signals with the terrestrial ^{26}Mg/^{24}Mg and ^{44}Ca/^{40}Ca ratios measured in the spinel and perovskite standards, respectively. This procedure is strictly speaking not correct because the intrinsic initial ^{26}Mg/^{24}Mg and ^{44}Ca/^{40}Ca ratios, i.e., the ratios without contributions from ^{26}Al and ^{44}Ti decay cannot be considered to be normal. However, in essential all cases, because of large Al/Mg and Ti/Ca ratios, the radiogenic contributions dominate. For Mg we can estimate the intrinsic anomaly in the ^{26}Mg/^{24}Mg ratio from the ^{25}Mg/^{24}Mg ratio. These issues have been discussed before (Zinner et al. 1991; Nittler et al. 1996). Deviations from the inferred ^{26}Al/^{27}Al and ^{44}Ti/^{48}Ti are probably small.

Another possibility of distorting these ratios is the presence of contamination by terrestrial Mg, Al, Ca, and Ti. Because the SiC-rich residues from Qingzhen also contain spinel, contamination is more likely to be an issue for Mg and Al than for Ca and Ti. Admixture of Mg with terrestrial isotopic ratios does not affect the inferred ^{26}Al/^{27}Al ratios. It reduces both the measured ^{26}Mg/^{24}Mg and Al/^{24}Mg ratio in the same way so that the ^{26}Al/^{27}Al ratio remains the same. The situation is different for contamination with Al. Any addition of non-intrinsic Al reduces the inferred ^{26}Al/^{27}Al ratio. Although we tried to avoid spinel grains, the possibility of their presence means that all ^{26}Al/^{27}Al ratios are strictly speaking only lower limits.

An example of some of the difficulties encountered in these analyses is exhibited in Figure 3, which shows secondary ion signals of several isotopes and isotopic ratios as a function of measurement time during the analysis of grain 5A-551-24. The increase of the Si signal at the beginning of the measurement is an artifact that is a combination of preferential sputtering and the differences in ionization efficiencies of different elements during the time O from the primary beam is implanted into the sample. What complicates the situation is that the sample has previously been analyzed with a Cs beam, i.e., the sample contains implanted Cs. Since Cs easily gives off an electron, its presence affects the ionization efficiency of other elements. The ionization efficiency might even depend on the site of atoms. Note that right at the beginning of the run, the behavior of the ^{26}Mg signal differs from that of the other Mg isotopes, probably reflecting the fact that the ^{26}Mg signal is dominated by radiogenic ^{26}Mg, derived from the decay of ^{26}Al. Thus, ion signals should be taken as reflecting the composition of the grain only after removal of Cs and implantation of O at around 200 s.

What is unexpected is that the ^{26}Mg/^{24}Mg and ^{26}Mg*/Al ratios vary during the measurement. The ^{26}Mg*/Al ratio (which within the Mg/Al sensitivity factor is the same as the ^{26}Al/^{27}Al ratio) varies from 0.058 at 200 s to a maximum of 0.19 at 600 s (corresponding to a variation from 0.044 to 0.15 for ^{26}Al/^{27}Al). The ^{26}Al/^{27}Al ratio derived from the counts obtained from the whole grain is 0.066. On the face of it, one might conclude that the ^{26}Al/^{27}Al ratio varies throughout the grain. However, this conclusion does not include the possibility of contamination. What makes us suspicious is the fact that the Mg concentration and the Mg/Al ratio in the grain are unusually high and the fact that the maximum of the inferred ^{26}Al/^{27}Al ratio occurs at a place where there is a dip in the ^{24}Mg and Al signals (Figure 3). In order to test whether contamination could account for the apparent variation in ^{26}Al/^{27}Al, we assumed a constant

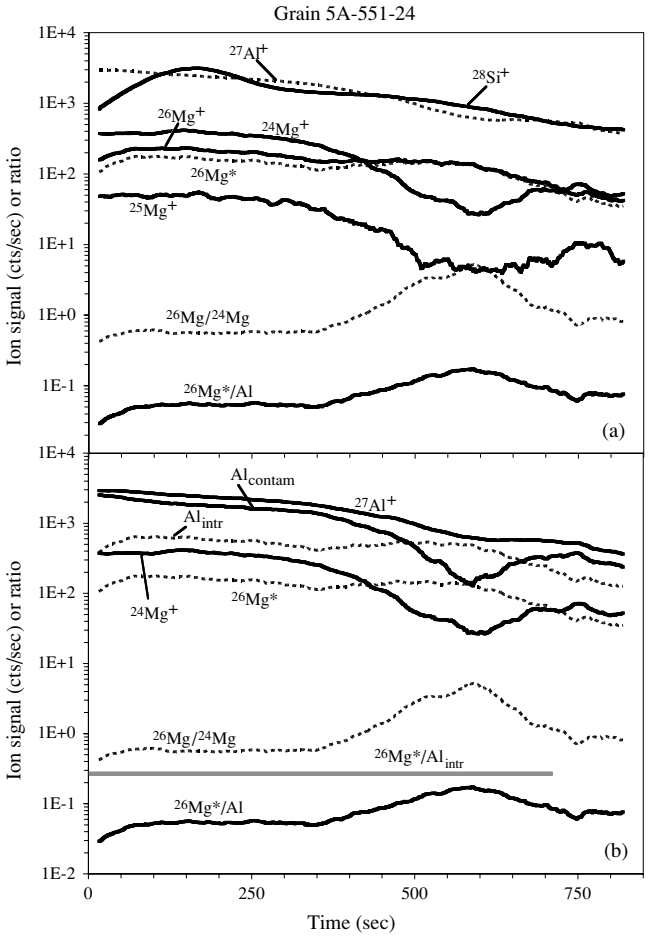

Figure 3. Depth profiles of ion signals and of isotopic ratios in grain 5A-551-24. In order to reduce scatter, we plot running averages over ten measurements. ^{26}Mg* denotes the radiogenic excess of ^{26}Mg due to the decay of ^{26}Al. In panel (a), it can be seen that radiogenic ^{26}Mg constitutes most of the ^{26}Mg signal. The apparent ^{26}Mg*/Al ratio is the same as the inferred initial ^{26}Al/^{27}Al ratio and varies as a function of depth. In panel (b), we assume that the initial ^{26}Al/^{27}Al was constant throughout the grain (horizontal line labeled ^{26}Mg*/Al$_{intr}$) and calculate the corresponding original Al content (Al$_{intr}$) and a contamination component (Al$_{contam}$) that would explain the apparent variation in the ^{26}Mg*/Al ratio. See the text for a more detailed discussion.

^{26}Al/^{27}Al ratio and calculated the corresponding intrinsic Al concentration, assuming that the remaining Al derives from contamination. The lower panel of Figure 3 shows this for an assumed ^{26}Mg*/Al ratio of 0.275 (corresponding to an ^{26}Al/^{27}Al ratio of 0.21). As can be seen, the calculated Al contamination is quite parallel to the ^{24}Mg signal, indicating a rather constant Al/Mg ratio for the contamination. Since contamination is likely for this grain, we cannot claim that its ^{26}Al/^{27}Al ratio is heterogeneous. Another consequence is that the true ^{26}Al/^{27}Al of the grain is much higher (0.21) than what we obtain from the total counts (0.066).

A possible problem with this scenario is that the Al/Mg ratio inferred for the contamination is ~5.6, much higher than the atomic Al/Mg ratio of 2 for spinel ($MgAl_2O_4$), the most likely mineral other than SiC to be present in the analyzed residue. Corundum (Al_2O_3) and hibonite ($CaAl_{12}O_{19}$), the other oxide phases that could be present, are expected to have much higher Al/Mg ratios, and silicates, which could have an Al/Mg ratio of 5.6, should have been removed by the chemical treatment. Furthermore, before the Mg–Al analysis, grain 5A-551-24 was examined in the SEM and no obvious adhering grain could

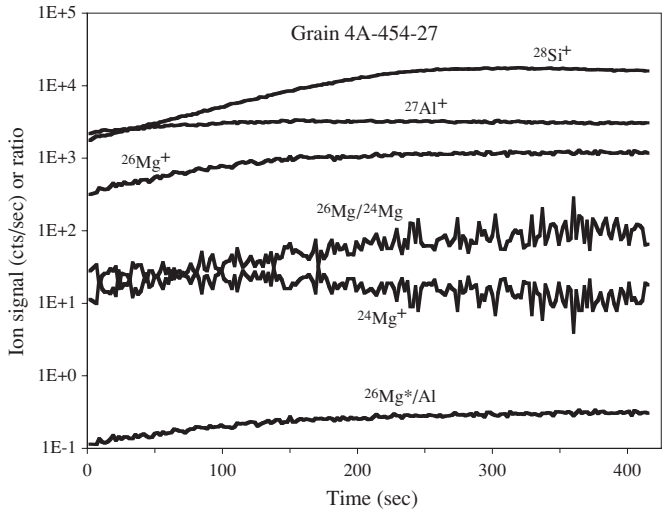

Figure 4. Depth profiles of ion signals and isotopic ratios in grain 4A-454-27. The different rates of increase of the ^{24}Mg, ^{26}Mg, ^{27}Al, and ^{28}Si are attributed to implantation effects at the beginning of the SIMS analysis. See the text for details.

be seen in the image. Thus, we cannot absolutely rule out heterogeneous ^{26}Al/^{27}Al in the grain. Still, the fact that the depth profile of the Al signal inferred for extraneous Al from the assumption of uniform ^{26}Al/^{27}Al mimics the depth profiles of ^{24}Mg and ^{25}Mg (i.e., the isotopically normal Mg) appears to be too much of a coincidence and contamination seems to be a more likely proposition.

Even in the absence of obvious contamination, surface effects in the ionization efficiency can lead to apparent variation in the inferred ^{26}Al/^{27}Al ratio. An example is shown in Figure 4. As is seen also in other grains, in grain 4A-454-27 the Si signal rises slowly, the ^{26}Mg signal less slowly, the Al signal even less so, and the ^{24}Mg signal not at all. In this grain, the Al/^{24}Mg ratio is much higher than in grain 5A-551-24 and the ^{26}Mg signal is almost entirely of radiogenic origin. But because of its slower rise than the Al signal, the inferred ^{26}Al/^{27}Al ratio apparently varies from 0.105 to 0.237. Again, the higher ratio is most likely the correct one.

3. RESULTS

3.1. Isotopic Compositions

Elemental and isotopic compositions of 10 SiC-X1, 8 SiC-X2, and 5 Si_3N_4 grains are given in Table 1. The C, N, and Si isotopic ratios in the table are taken from our previous analysis of these grains (Lin et al. 2002). All grains analyzed for Mg show normal ^{25}Mg/^{24}Mg ratios within measurement errors, but large excesses of ^{26}Mg, indicating the initial presence of short-lived ^{26}Al, with the inferred ^{26}Al/^{27}Al ratios ranging from 6.3 × 10^{-3} to 0.31. Figure 5 shows the ^{26}Al/^{27}Al ratio plotted versus ^{12}C/^{13}C and δ^{29}Si/^{28}Si. Together with the results of this study, we also plot the results of previous studies of X grains from other meteorites (Amari et al. 1992 and unpublished; Hoppe et al. 1994, 1996, 2000; Nittler 1996; Nittler et al. 1996; Nittler & Hoppe 2005; Huss et al. 1997; Henkel et al. 2007; Zinner et al. 2007). The X1 grains of our study appear to have on average somewhat higher ^{26}Al/^{27}Al ratios than the X2 grains. However, if we consider all grains, 45 out of 63 (71%) X1 grains and 17 out 27 (63%) of X2 grains have ^{26}Al/^{27}Al ratios greater than 0.1, a difference that is statistically not significant. There are no obvious strong correlations between ^{26}Al/^{27}Al and either

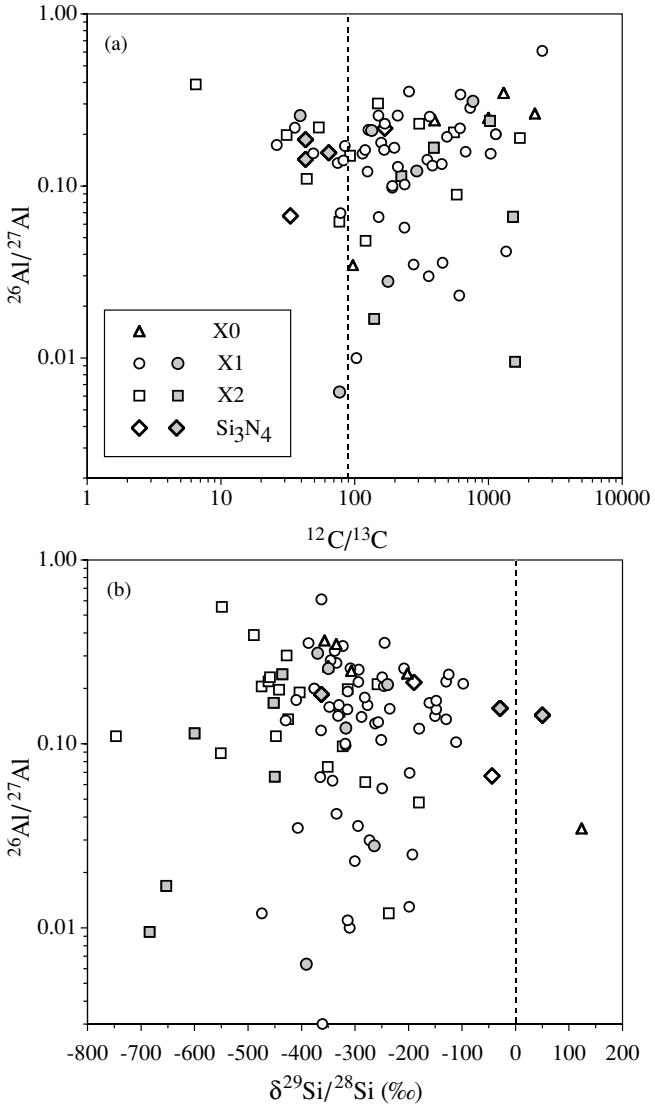

Figure 5. Inferred initial ^{26}Al/^{26}Al ratios of different subtypes of X grains as a function of the ^{12}C/^{13}C ratio (a) and the ^{29}Si/^{28}Si ratio (b). The upper limits of the ^{26}Al/^{26}Al ratio tend to increase with increasing ^{12}C/^{13}C ratios and decreasing ^{29}Si/^{28}Si ratios. The numbers of grains in the two plots are not identical because not all grains had their C and Si isotopic ratios measured.

^{12}C/^{13}C or δ^{29}Si/^{28}Si. Except for one special grain with an unusually low ^{12}C/^{13}C ratio (Nittler & Hoppe 2005), the upper cutoff for ^{26}Al/^{27}Al increases with increasing ^{12}C/^{13}C (Figure 5(a)) and with decreasing δ^{29}Si/^{28}Si (Figure 5(b)), but more analyses are needed to make this a firm observation. In Figure 5(b), the δ^{29}Si/^{28}Si values of X2 grains are smaller but this is a consequence of the grains' definition based on their Si isotopic ratios (Figures 1 and 2).

Four SiC-X1 grains and four SiC-X2 grains have ^{44}Ca excesses of more than 2σ (Table 1). No excess of ^{44}Ca was detected for all four Si_3N_4 grains within the analytical errors. Although we have not obtained isotopic ratios for ^{42}Ca and ^{43}Ca, we assign a radiogenic origin to these ^{44}Ca excesses. The O/C and O/Ne zones have high ^{44}Ca and low ^{40}Ca abundances (Rauscher et al. 2002) that would give large ^{44}Ca excesses. However, these zones are so rich in oxygen that any admixture from these layers that would reproduce the ^{44}Ca excesses in our grains results in C/O ratios of much less than 1, i.e., in conditions that are not conducive to the condensation of SiC (Ebel & Grossman 2001). Still, we caution the reader that ^{44}Ca excesses of less than 200‰

Table 1
Isotopic and Elemental Data on Type X SiC and Si_3N_4 Grains

Grain Label	Type	$^{12}C/^{13}C$	$^{14}N/^{15}N$	$\delta^{29}Si/^{28}Si$ (‰)	$\delta^{30}Si/^{28}Si$ (‰)	$^{26}Al/^{27}Al$ (×1000)	$\delta^{44}Ca/^{40}Ca$ (‰)	$^{44}Ti/^{48}Ti$ (×1000)	$\delta^{46}Ti/^{48}Ti$ (‰)	$\delta^{47}Ti/^{48}Ti$ (‰)	$\delta^{49}Ti/^{48}Ti$ (‰)	Al[a] (%)	Mg[a] (%)	Ca[a] (ppm)	Ti[a] (ppm)	V[a] (ppm)
4A-277-18	X1	77 ± 4	102 ± 10	−391 ± 14	−510 ± 12	6.3 ± 0.4	146 ± 66	3.5 ± 1.6	−79 ± 51	−133 ± 51	240 ± 72	12.5[b]	2.17[b]	1117	1088	22.6
4A-300-6	X1	556 ± 42	80 ± 4	−345 ± 9	−549 ± 8		82 ± 61		49 ± 182	−124 ± 167	888 ± 309			213	16	0.2
4A-430-14	X1	101 ± 3	136 ± 5	−186 ± 10	−235 ± 11		39 ± 26		−40 ± 53	−80 ± 53	305 ± 75			2774	385	2.7
4A-438-25	X1	134 ± 11	70 ± 3	−239 ± 15	−362 ± 14	210 ± 6						5.8	0.08			
4A-454-27	X1	39 ± 1	24.9 ± 0.6	−350 ± 12	−439 ± 11	257 ± 7	122 ± 57	55 ± 26	314 ± 215	230 ± 210	897 ± 315	3.73	0.02	845	48	1.4
4A-461-5	X1	101 ± 3	22.6 ± 0.5	−96 ± 11	−189 ± 11		48 ± 45		−6 ± 25	−67 ± 25	72 ± 32			1492	3196	27.4
4A-482-20	X1	765 ± 147	68 ± 3	−370 ± 23	−493 ± 20	311 ± 82	−104 ± 175		195 ± 350	21 ± 325	1180 ± 598	4.98	0.0003	816	215	18.6
5A-188-1	X1	357 ± 9	81 ± 2	−284 ± 3	−443 ± 3		65 ± 19	1.2 ± 0.3	−3 ± 17	−16 ± 16	155 ± 21			1132	1432	23
5A-396-3	X1	177 ± 6	138 ± 7	−264 ± 6	−389 ± 5	28 ± 1	32 ± 84		32 ± 169	40 ± 179	144 ± 217	1.43	0.02	434	76	1.9
5A-564-14	X1	291 ± 8		−317 ± 6	−487 ± 5	122 ± 2	1225 ± 297	5.7 ± 1.4	−72 ± 71	−137 ± 71	691 ± 124	1.09	0.04	62	306	8.9
4A-134-9	X2	391 ± 27	39 ± 1	−452 ± 9	−387 ± 11	167 ± 2	4977 ± 634	25.6 ± 2.5	138 ± 98	−141 ± 85	1148 ± 173	0.5	0.07	42	189	3.3
4A-219-27B	X2	223 ± 39	102 ± 10	−600 ± 18	−459 ± 20	114 ± 10	136 ± 124		−9 ± 46	15 ± 48	5 ± 55	2.55	0.03	653	3173	88.3
5A-80-7	X2	1026 ± 65	88 ± 2	−436 ± 5	−494 ± 5	239 ± 2	88 ± 32	7.4 ± 2.7	22 ± 48	−62 ± 48	768 ± 83	7.65	0.11	1184	331	7.9
5A-117-3	X2	1581 ± 102	116 ± 11	−684 ± 3	−490 ± 4	9.5 ± 0.7	7584 ± 571	935 ± 129	848 ± 557	116 ± 342	2517 ± 814	0.28	0.04	55	11	1.5
5A-247-4	X2	95 ± 2	52 ± 2	−469 ± 5	−581 ± 5		383 ± 105	46 ± 17	72 ± 173	17 ± 178	118 ± 216			37	7	0.1
5A-283-8	X2	1848 ± 378	6.9 ± 0.2	−540 ± 9	−308 ± 11		18 ± 127		−242 ± 176	−180 ± 196	−396 ± 188			1307	345	7.2
5A-425-14	X2	140 ± 10	97 ± 10	−653 ± 6	−446 ± 7	17 ± 2						0.91	0.07			
5A-551-24	X2	1528 ± 270	46 ± 2.0	−450 ± 8	−348 ± 9	66 ± 1						15.1[b]	1.74[b]			
4A-107-16	Si_3N_4	43 ± 5	26 ± 1	50 ± 23	−174 ± 20	143 ± 4	72 ± 40		342 ± 147	5 ± 126	255 ± 165	0.92	0.02	4651	295	4.5
4A-194-20	Si_3N_4	64 ± 20	189 ± 18	−29 ± 14	−42 ± 15	156 ± 4	63 ± 123		397 ± 740	56 ± 635	504 ± 904	1.47	0.23	3896	70	2.4
4A-280-3	Si_3N_4	67 ± 2	64 ± 1	−165 ± 10	−262 ± 10		28 ± 14		97 ± 38	71 ± 39	150 ± 46			7860	306	2.7
4A-306-21	Si_3N_4	43 ± 9		−363 ± 22	−445 ± 20	186 ± 21						1.54	0.03			
5A-339-5	Si_3N_4	221 ± 48	127 ± 8	−442 ± 9	−436 ± 8		−223 ± 92		1819 ± 1085	2284 ± 1236	170 ± 748			7777	92	7.4

Notes. All errors are 1σ.
[a] Elemental concentrations are based on total counts, without taking into account any surface effects as discussed in the text. For Mg, Ca, and Ti they are based on ^{24}Ma, ^{40}Ca, and ^{48}Ti under the assumption of normal isotopic ratios.
[b] A substantial amount might be contamination. See Figure 3 and discussion in the text.

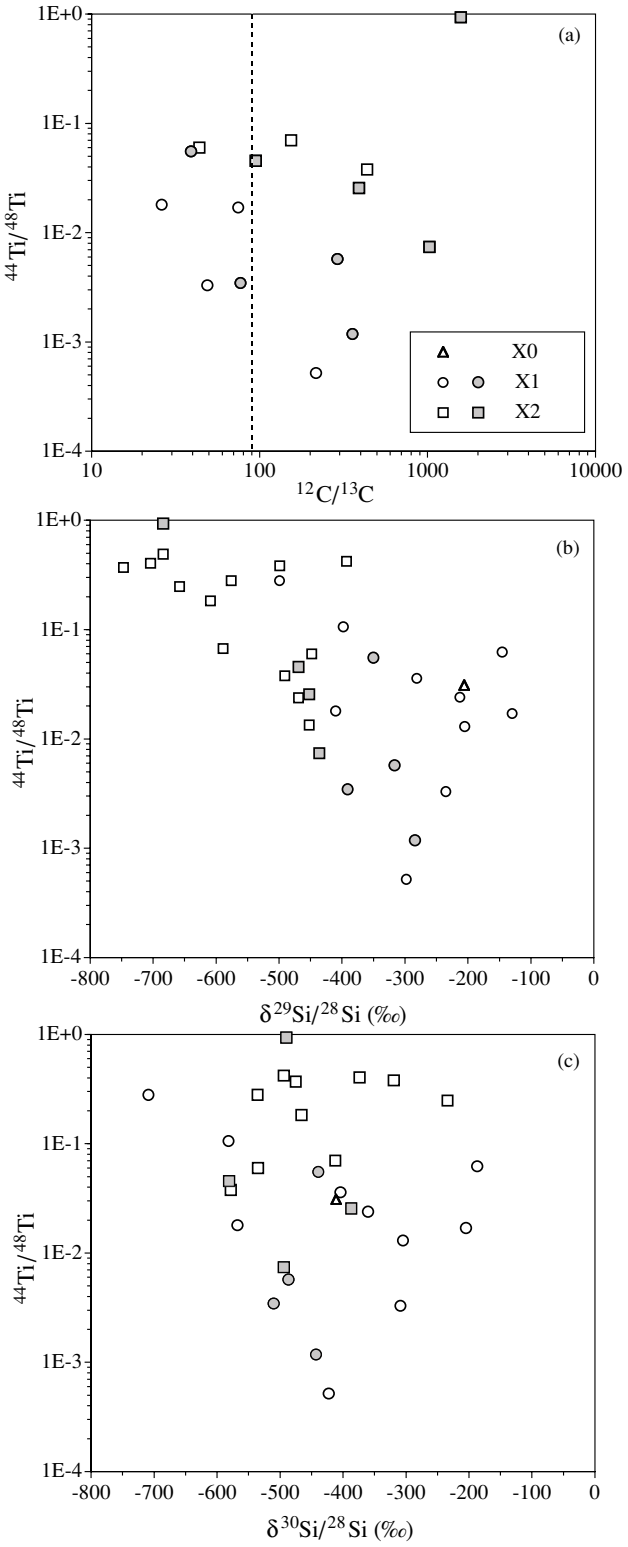

Figure 6. Inferred initial ^{44}Ti/^{48}Ti ratios of different subtypes of X grains as a function of the C and Si isotopic ratios. Type X2 grains have the highest ^{44}Ti/^{48}Ti ratios and there is an overall negative correlation between these ratios and the ^{29}Si/^{28}Si ratios, with X2 grains having the smallest ^{29}Si/^{28}Si ratios and largest ^{44}Ti/^{48}Ti ratios. No such correlations are apparent between ^{44}Ti/^{48}Ti and ^{12}C/^{13}C or ^{30}Si/^{28}Si. There are fewer data points in (a) because not all X grains had their C isotopic ratios measured.

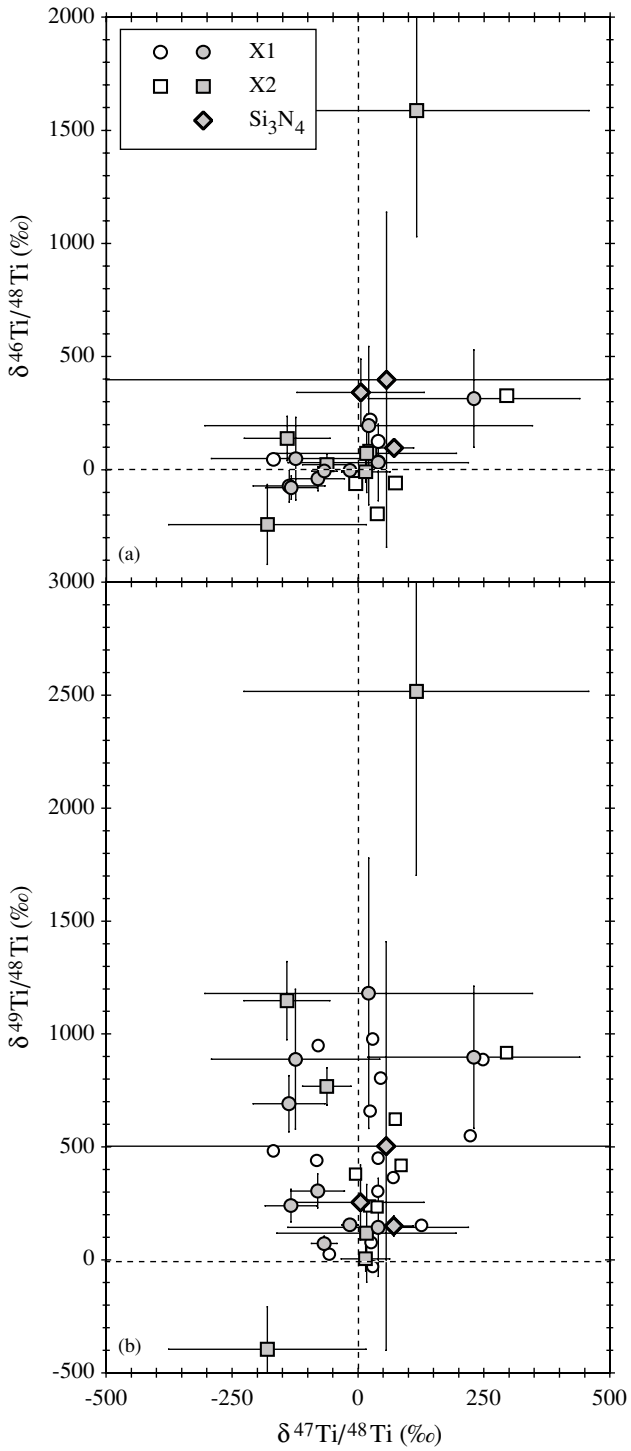

Figure 7. Titanium isotopic ratios of different subtypes of X grains. 1σ errors are shown only for the grains of this study. Data from other studies are plotted if at least one ratio is anomalous by 1.5σ.

could reflect contributions from the O-rich SN zones if these grains can condense in a gas with C < O. Figure 6 is a plot of inferred ^{44}Ti/^{48}Ti versus $\delta^{29,30}$Si/^{28}Si of our data and those of other investigators (Amari et al. 1992 and unpublished; Hoppe et al. 1996, 2000; Nittler et al. 1996; Besmehn 2001; Besmehn & Hoppe 2003). The ^{44}Ti/^{48}Ti versus δ^{29}Si/^{28}Si plot (Figure 6(b)) exhibits a clear negative correlation between these two ratios. It also shows that, although there is some overlap, X2 grains on average have much larger ^{44}Ti/^{48}Ti ratios than X1 grains. The ratio of 0.94 in grain 5A-117-3 is the highest value reported to date.

Our Ti isotopic ratios are plotted in Figure 7 together with data from other investigations (Amari et al. 1992 and unpublished;

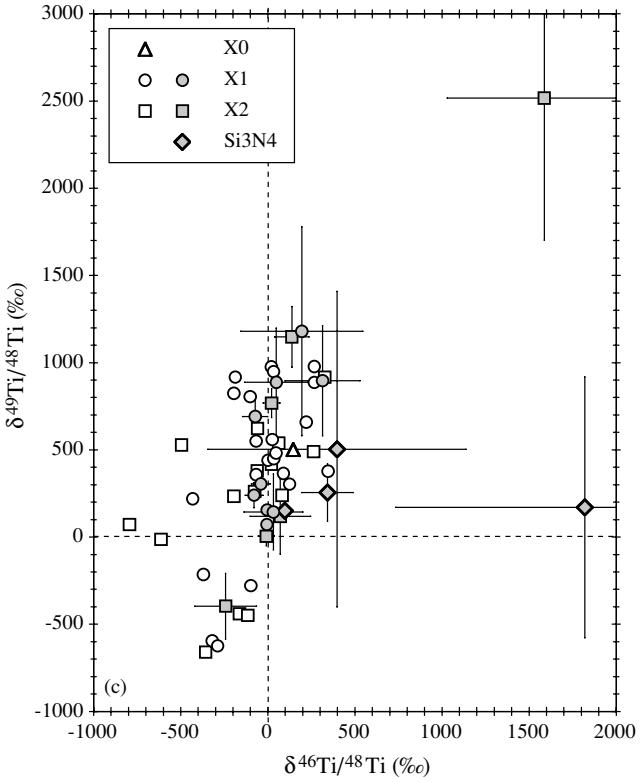

Figure 7. (Continued)

Nittler et al. 1996; Hoppe & Besmehn 2002; Nittler & Hoppe 2005). The $^{46}Ti/^{48}Ti$ and $^{47}Ti/^{48}Ti$ ratios of most of our grains are normal. Two Si_3N_4 grains have ^{46}Ti excesses larger than 2σ and two SiC X1 grains ^{47}Ti deficits exceeding 2σ. The situation is completely different for ^{49}Ti, for which we find large excesses (Table 1 and Figure 7(b)). Grain 5A-283-8 has ^{46}Ti and ^{49}Ti deficits, but the anomalies in this grain are marginal. Figure 7(c) shows that quite a few previously measured X grains have substantial deficits in ^{46}Ti and ^{49}Ti. These grains do not show up in Figures 7(a) and 7(b) because their $^{47}Ti/^{48}Ti$ ratios had not been measured. Hoppe & Besmehn (2002) have argued on the basis of a correlation between ^{49}Ti excesses and the V/Ti ratios in X grains for a radiogenic origin of these excesses from the decay of short-lived ($T_{1/2} = 332$ d) ^{49}V. In Figure 8, we plot $\delta^{49}Ti/^{48}Ti$ versus the $^{51}V/^{48}Ti$ ratio together with the data by Hoppe & Besmehn (2002) and a few unpublished measurements by Amari. We observe a general correlation for our data, although there is a lot of scatter. However, the best-fit (dashed) line through our data has a much larger slope than the (solid) line through the data points of Hoppe & Besmehn (2002). One glaring difference is that, on average, our $^{51}V/^{48}Ti$ ratios are much smaller. If ^{49}Ti has indeed a radiogenic origin (we shall return to this issue in the next section), our data imply a higher $^{49}V/^{51}V$ ratio than those by Hoppe & Besmehn (2002).

3.2. Elemental Compositions

The Al and Mg contents of all X grains of this study cover a large range as do the Al/Mg ratios (Table 1). Magnesium does not condense easily into SiC (Lodders & Fegley 1995, 1997) and Mg concentrations of all types of SiC grains are lower than Al concentrations (Amari et al. 1995). The Mg concentrations of two X grains of this study (4A-277-18 and 5A-551-24) are much higher than those of the other grains. These two grains have also the highest Al contents, and for the second grain we argued that

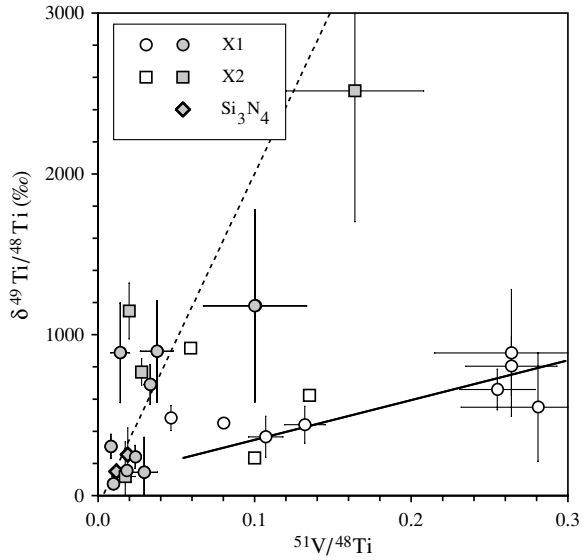

Figure 8. $^{49}Ti/^{48}Ti$ ratios of different subtypes of X grains as a function of the $^{51}V/^{48}Ti$ ratio. The solid line is a correlation line through the data obtained by Hoppe & Besmehn (2002), the broken line a correlation line through our data.

contamination could possibly account for the high Al and Mg concentrations, in which case the true inferred $^{26}Al/^{27}Al$ ratio could be much higher (Figure 3). In contrast to grain 5A-551-24, the Al and Mg signals are essentially constant throughout the analysis of grain 4A-277-18 but, again, we cannot exclude contamination to account for most of the Al and Mg measured. Another grain with a relatively low Al/Mg ratios is grain 4A-134-9; however, both the Al and Mg concentrations are low. This grain also has a large ^{26}Mg excess (Figure 9(a)) and the inferred $^{26}Al/^{27}Al$ ratio is 0.17 (Table 1). The situation is similar for X Si_3N_4 grain 4A-194-20. A special case of the opposite extreme is represented by grain 4A-482-20, which has an extremely low content of normal Mg (Table 1) and in which essentially all of its Mg is radiogenic ^{26}Mg. During the analysis of this grain, we obtained only 29 counts of ^{24}Mg, compared to 131,000 counts of ^{26}Mg, resulting in a $^{26}Mg/^{24}Mg$ ratio of 4500 (the normal ratio is 0.139). We cannot observe any obvious differences between X1 and X2 grains either in their Al and Mg contents or their Al/Mg ratios.

The Ca, Ti, and V concentrations also cover large ranges (Table 1 and Figure 10). We cannot observe any obvious correlation between the Ca and Ti abundances, as well as no differences between X1 and X2 grains. Silicon nitride X grains have higher Ca abundances than any of the SiC X grains (Figure 10(a)). There is a clear difference in the distribution of Ca, Ti, and V inside the grains. Figures 9(b) and 11 show depth profiles of the ion signals of selected isotopes of two SiC grains during the NanoSIMS analysis as the primary ion beams sputter material from the grains. Titanium appears to reside in subgrains, an observations made previously for an SiC X grain (Besmehn & Hoppe 2003), but also for mainstream grains (Gyngard et al. 2006). Transmission electron microscope (TEM) studies of SiC grains identified TiC subgrains within a mainstream grain (Bernatowicz et al. 1992) and an X grain (Hynes et al. 2006). In contrast to Ti, Ca is more uniformly distributed (Figures 9(b) and 11) throughout the grains as are Al and Mg (Figure 9(a)). The spatial distribution of Ti and Ca in X grains is similar to that of Fe and Ni, where Fe resides in subgrains, whereas Ni is fairly uniformly distributed throughout the SiC grains (Marhas et al. 2008).

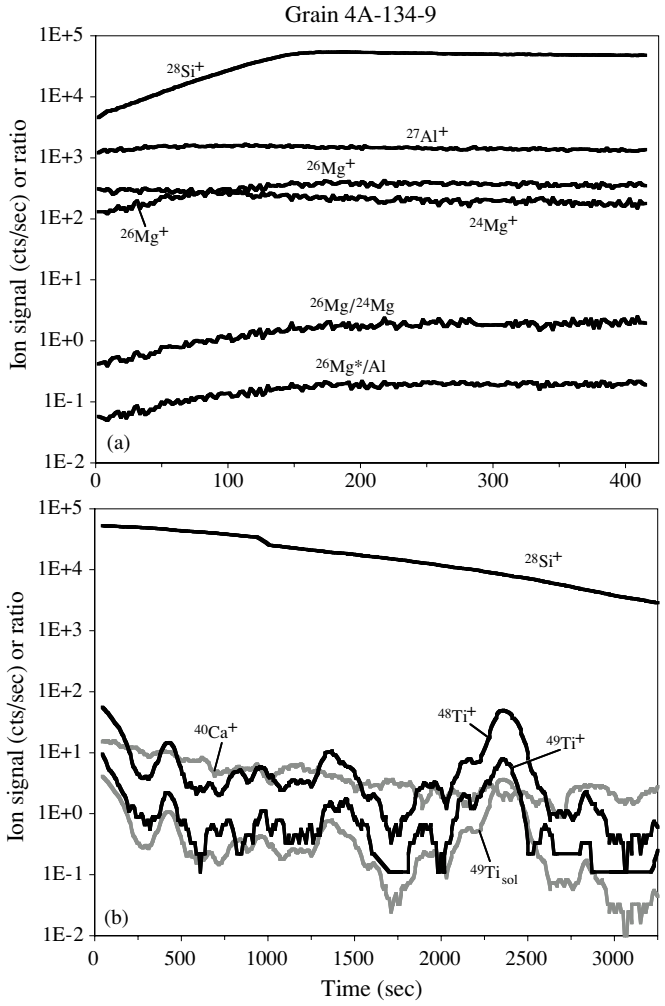

Figure 9. Depth profiles of ion signals and isotopic ratios in grain 4A-134-9. Panel (a) displays traces of Mg, Al, and Si, panel (b) of Si, Ca, and Ti. The measurements of (a) were made before those of (b). Because of the low ion signal in panel (b), we plotted running averages over ten measurements. As for grain 4A-454-27 (Figure 4), the slow initial increase of the ^{28}Si signal (and to a lesser extent that of ^{26}Mg in (a)) is an implantation effect of the primary beam. Because O was already implanted when the Ca–Ti profile was obtained, there is no such increase in (b) and the ^{28}Si signal decreases as the grain is sputtered away. The Ti signals vary strongly, indicating the presence of Ti-rich subgrains. The ^{49}Ti$_{sol}$ line is the signal expected for a solar ^{49}Ti/^{48}Ti ratio. This grain clearly has a ^{49}Ti excess.

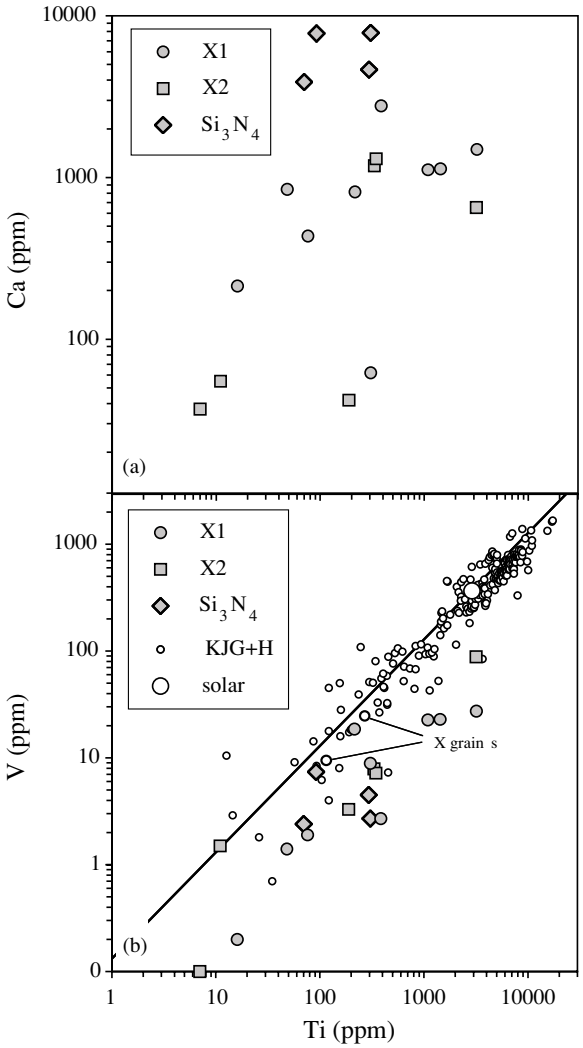

Figure 10. Concentrations of Ca, Ti, and V measured in X grains. Panel (b) shows also Ti and V abundances previously measured in the KJG and KJH size fractions of Murchison SiC grains (Amari et al. 1995; Gyngard et al. 2006 and unpublished). Two X grains from the previous studies are indicated. The solid black line in panel (b) is a line with solar V/Ti ratio.

Vanadium and Ti abundances are fairly well correlated (Figure 10(b)). This is also shown in Figure 11, where V follows Ti in grain 4A-461-5; in grain 4A-134-9 (Figure 9(b)) the V signal was too low for determination of its spatial distribution. Grain 4A-461-5 has no ^{49}Ti excess, but grain 4A-134-9 does. In Figure 9(b), we plot a ^{49}Ti profile expected for a solar ^{49}Ti/^{48}Ti ratio in this grain. It can be clearly seen that the measured ^{49}Ti signal is higher. Figure 10(b) shows also Ti and V abundances previously measured in grains from Murchison SiC separates KJG and KJH (Amari et al. 1995; Gyngard et al. 2006 and unpublished). Most of these grains are mainstream grains; two X grains from KJH are indicated in the plot. The Ti and V abundances of our grains are not only lower than those of most KJG and KJH grains, but the V/Ti ratios are lower. Most KJG and KJH grains have V/Ti ratios close to the solar ratio (the solid line in Figure 10(b)), and this has been interpreted that both Ti and V go into SiC during its condensation (Amari et al. 1995; Lodders & Fegley 1995, 1999). In contrast, our X grains fall below this line. It has been noted before (Amari et al. 1995) that X grains have lower concentrations of refractory trace elements than mainstream grains. However, we have no satisfactory explanation why the V/Ti ratios of our X grains are not only lower than those of mainstream grains but, as already pointed out in the previous section, also lower than those of the X grains from Murchison measured by Hoppe & Besmehn (2002). We believe that we can exclude an experimental artifact and we still see a general correlation between the Ti and V abundances. Even the ^{51}V/^{48}Ti ratios measured by Hoppe and Besmehn span a factor of almost 3, and 4 of their grains have higher than solar ratios (^{51}V/^{48}Ti$_{solar}$ = 0.16). In addition, ratios measured in several X grains by Amari (unpublished) are lower than 0.1 (open symbols in Figure 8). On the other hand, it is difficult to believe that X grains from Qingzhen have different V/Ti ratios than X grains from Murchison. This issue still needs further exploration.

4. DISCUSSION

Our measurements of X grains from Qingzhen show high inferred ^{26}Al/^{27}Al and ^{44}Ti/^{48}Ti ratios, in agreement with previous analyses of X grains from other meteorites (see references cited in the previous section). They also reveal large

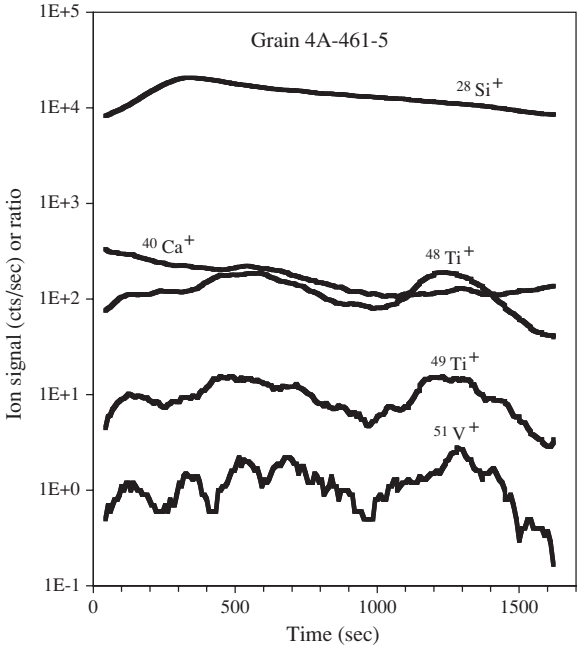

Figure 11. Depth profiles of ion signals (running averages over ten analyses) in grain 4A-461-5. Similar to grain 4A-134-9, the variation in the Ti signals indicates the presence of Ti-rich subgrains. This grain has normal Ti isotopic ratios. Vanadium appears to have the same spatial distribution as Ti, markedly different from that of Ca.

excesses in ^{49}Ti, possibly from the decay of short-lived ^{49}V (Hoppe & Besmehn 2002). The isotopic properties of X grains and their stellar origin have been discussed previously (see section on Type X Grains in Zinner 2007, and references therein) and we do not want to repeat that discussion. Here we first discuss the possible radiogenic origin of ^{49}Ti excesses and then concentrate of the different classes (X0, X1, and X2) of SiC X grains and the question whether or not differences of other isotopic systems can be found among these classes.

4.1. Initial Presence of Short-lived ^{49}V?

Hoppe & Besmehn (2002) argued for a radiogenic origin of the ^{49}Ti excesses observed in X grains from the decay of ^{49}V on the basis of a correlation between ^{49}Ti excesses and the ^{51}V/^{48}Ti ratio (see Figure 8 and the discussion in the previous section). Travaglio et al. (1999) also argued for the initial presence of ^{49}V in low-density graphite grains, which are believed to have a SN origin. That ^{49}V is present during grain formation is expected because ^{49}V is produced in the Si/S zone, which is rich in ^{28}Si and where also ^{44}Ti is produced (Woosley & Weaver 1995; Timmes et al. 1996; Rauscher et al. 2002, see Figures 12(a)–12(c)). On the other hand, a strict correlation between ^{49}Ti excesses and ^{51}V/^{48}Ti would correspond to a constant ^{49}V/^{51}V ratio, which should not be expected. First, even if all ^{49}Ti excesses are indeed of radiogenic origin, the final ^{49}V/^{51}V ratio depends on how much ^{49}V from the Si/S (and possibly the O/Si zone, see Figures 12(b) and 12(c)) is mixed into C-rich regions. Furthermore, the ^{49}V abundance is not constant in these interior SN regions (Figures 12(a)–12(c)). We want to point out that in Figures 12(a)–12(c) and in later figures showing theoretical SN predictions, stable isotopes are shown after the decay of short-lived precursors. For example, ^{48}Ti is taken after the decay of ^{48}Cr and ^{48}V, ^{49}Ti after the decay of ^{49}V, and ^{51}V after the decay of ^{51}Cr. The radionuclides ^{48}V and ^{51}Cr have short enough half-lives (16 and 28 d, respectively) that they most likely decayed before grain formation. In contrast, ^{49}V has a

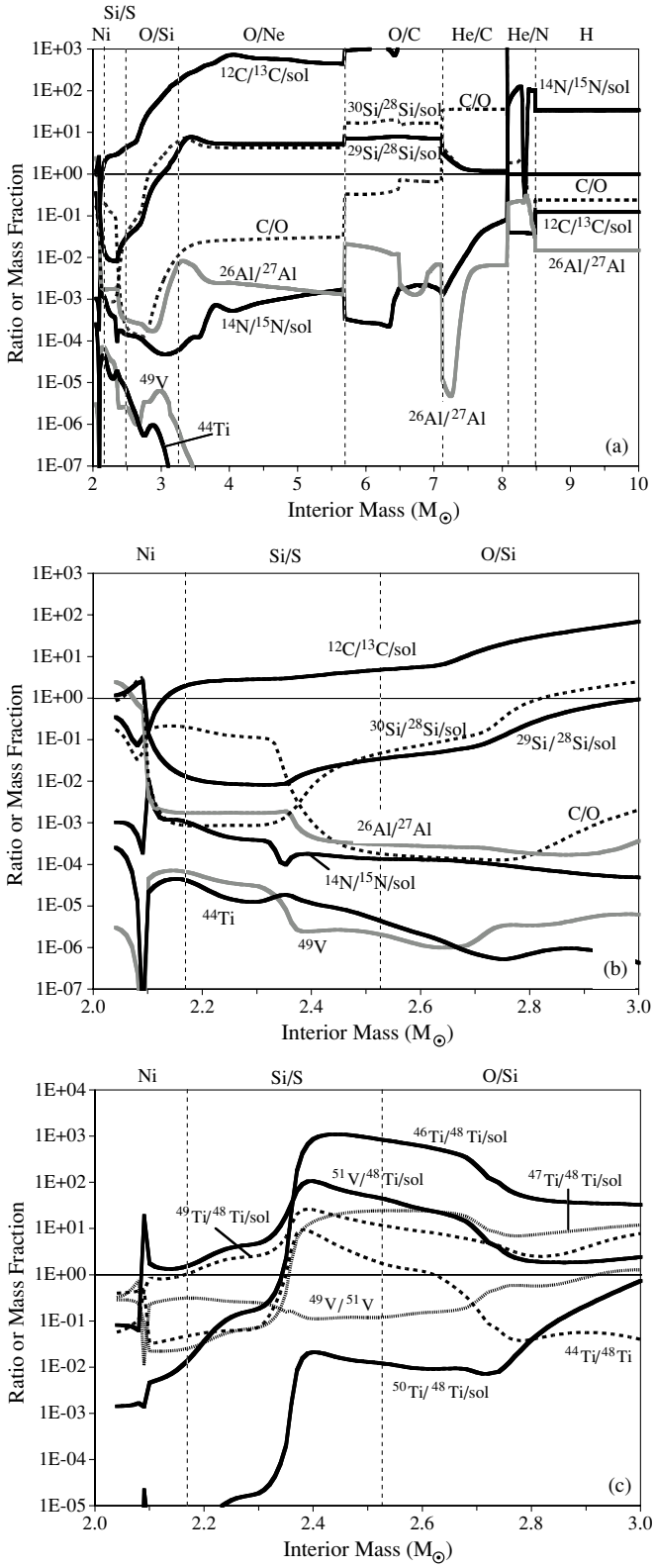

Figure 12. Theoretical predictions of isotopic ratios and isotopic abundances from the 25 $M_\odot$ SN model by Rauscher et al. (2002). The isotopic ratios of C, N, Si, Ti, and V are normalized to the solar ratios. C/O > 1, believed to be required for SiC condensation, is found in the He/C zone and the inner part of the He/N zone (panel (a)). The short-lived radioisotopes ^{44}Ti and ^{49}V are produced in the interior zones (panels (b) and (c)). The isotopic ratios, specifically the Ti ratios in panel (c), are obtained after the decay of the short-lived nuclides such as ^{48,51}Cr and ^{48,49}V, except where ^{44}Ti and ^{49}V are plotted.

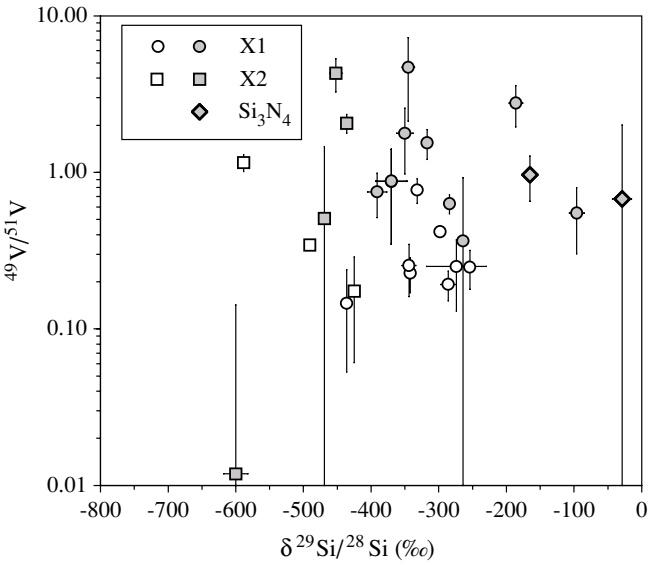

Figure 13. Inferred initial $^{49}V/^{51}V$ ratios of different subtypes of X grains as a function of the $^{29}Si/^{28}Si$ ratio.

half-life of 336 d, and a substantial fraction probably condensed into SiC grains as ^{49}V. Thus, elemental fractionation between V and Ti potentially may play a role. Finally, the inferred $^{44}Ti/^{48}Ti$ ratios in X grains vary over a wide range and are roughly correlated with the $^{29}Si/^{28}Si$ ratios (Figure 6(b)). In order to see whether this is the case also for $^{49}V/^{51}V$, we plot this ratio, calculated under the assumption that the whole ^{49}Ti excess is of radiogenic origin, against the $^{29}Si/^{28}Si$ ratio (Figure 13). In contrast to the $^{44}Ti/^{48}Ti$ ratio, the $^{49}V/^{51}V$ ratio in the grains does not show any obvious correlation with $^{29}Si/^{28}Si$, nor is this ratio systematically higher in X2 grains. However, we note that the $^{44}Ti/^{48}Ti$ versus $^{29}Si/^{28}Si$ correlation mainly depends on X2 grains with $\delta^{29}Si/^{28}Si < -500‰$, whereas there are only two $^{49}V/^{51}V$ data points with such $\delta^{29}Si/^{28}Si$ values, one with a large error (Figure 13).

This difference between ^{44}Ti and ^{49}V is also shown in Figure 14(a), where we plot the $^{49}V/^{51}V$ ratio versus the $^{44}Ti/^{48}Ti$ ratio. Unfortunately, data on both these ratios are limited. Although the lack of correlation between these ratios is not unexpected because their relative abundances vary throughout the inner zones (Figure 12(c)), the relative abundances in the grains (Figure 10(b)) cannot easily be explained. In Figure 14(a), we also show as small diamonds both ratios predicted for the layers between 2.05 and 3.0 $M_\odot$ interior mass of the 25 $M_\odot$ SN model by Rauscher et al. (2002, henceforth RAU). Because in these layers C $\ll$ O, mixing with C-rich material is required and the diamonds should be taken only as reference points. Thus, in addition, we show lines representing isotopic ratios obtained by mixing various layers from the Ni, Si/S, and O/Si zones (indicated by the interior mass) with a mix of material from the He/N and He/C zones. The mixing is between layers at 7.6 $M_\odot$ (He/C zone) and 8.2 $M_\odot$ (He/N zone), and we have chosen a mix that gives $^{12}C/^{13}C = 100$. Such a mix has a $\delta^{49}Ti/^{48}Ti$ value of 522‰. Taking a more interior layer from the He/C zone or choosing a higher $^{12}C/^{13}C$ ratio would have resulted in an even higher $\delta^{49}Ti/^{48}Ti$ value. The mixing lines in Figure 14(a) are only for material with C > O. The two lines with material at 2.05 and 2.8 $M_\odot$ are not realistic, because these layers do not have large ^{28}Si excesses (see Figure 12(b)). It is seen in Figure 14(a) that most of our data points fall above the mixing lines. This would indicate that not all the ^{49}Ti excesses measured in the grains are due to the decay of ^{49}V, as was assumed for determining the $^{49}V/^{51}V$ ratios of the grains plotted in Figures 13 and 14(a). In Figure 14(a), we have also indicated, by gray data points (and arrows), the inferred $^{49}V/^{41}V$ ratios of our Qingzhen grains if the $^{51}V/^{48}Ti$ ratio of the grains were solar (0.16) instead of the much lower ratios we measured. This moves our data points closer to the mixing curves, although three points are still removed from the curves by at least a factor of 3. Grain 5A-117-3, with the highest inferred $^{44}Ti/^{48}Ti$ ratio, has already a close-to-solar $^{51}V/^{48}Ti$ ratio and its $^{49}V/^{41}V$ ratio does not change much.

However, the suspicion that ^{49}V-decay does not account for all the ^{49}Ti excesses measured in the grains is supported by other observations. The He/C zone has large excesses in ^{49}Ti from neutron capture. In the 25 $M_\odot$ RAU SN model, the ^{49}Ti excess varies from 1530‰ to 127,700‰ as one traverses the He/C zone from the outside to the inside. In order to explain the C and N isotopic ratios of X grains, material from the He/C zone (where $^{12}C/^{13}C$ ratios are high and $^{14}N/^{15}N$ ratios low) has to be mixed with the He/N zone (where the $^{26}Al/^{27}Al$ ratios are highest). Material from the He/C zones is also needed to explain the Fe and Ni isotopic ratios measured in X grains (Marhas et al. 2008). We have already pointed out that the He/N–He/C mix used for Figure 14(a) has a $\delta^{49}Ti/^{48}Ti$ value of 522‰. In Figure 14(b), we plot the $^{49}Ti/^{48}Ti$ ratios of the grains against their inferred $^{44}Ti/^{48}Ti$ ratios together with mixing curves obtained after mixing with layers from the Ni, Si/S, and O/Si zones as we did in Figure 14(a). It can be seen that for almost half the grains the ^{49}Ti excesses can be accounted for by neutron capture in the He/C zone and we do not need any contributions from ^{49}V decay. Our He/N–He/C mix has $^{12}C/^{13}C = 100$. Increasing this ratio requires admixture of more material from the He/C zone and results in higher $^{49}Ti/^{48}Ti$ ratios. For example, a He/N–He/C mix with $^{12}C/^{13}C = 400$ has a $\delta^{49}Ti/^{48}Ti$ value of 1039‰. In Figure 14(b), next to the data symbols, we show the $^{12}C/^{13}C$ ratios of the grains. Many of them are much higher than 100, implying higher $\delta^{49}Ti/^{48}Ti$ values for the He/N–He/C mix. Thus, only for a couple of grains do we seem to need a ^{49}V contribution. We thus conclude that the ^{49}Ti excesses in X grains must have contributions from both, admixture of material from the He/C zone and decay of ^{49}V from the interior zones. We note that, in contrast to ^{49}Ti, ^{44}Ca is not enhanced in the He/C zone relative to the He/N zone (RAU), thus, admixture of material from the He/C zone does not result in ^{44}Ca excesses. This makes it likely that ^{44}Ca excesses are due to ^{44}Ti decay, even when, as in our case, we do not have information on the other Ca isotopic ratios.

We can obtain more information about admixture from the inner SN zones from the Ti isotopic ratios of the grains. Figure 14(b) shows that the largest increase in the $^{49}Ti/^{48}Ti$ ratio comes from admixture from the Si/S layer at 2.4 $M_\odot$ interior mass because there the relative contribution from ^{49}V, i.e., the $^{49}Ti/^{48}Ti$ ratio after ^{49}V decay, is highest (see Figure 12(c)). However, the outer layer of the Si/S zone is extremely ^{46}Ti-rich with very high $^{46}Ti/^{48}Ti$ ratios. In Figure 14(c), we plot $^{46}Ti/^{48}Ti$ and $^{44}Ti/^{48}Ti$ ratios of grains and SN mixing curves. It is apparent that any admixture from the outer Si/S and inner O/Si zones from layers with $\geqslant$2.4 $M_\odot$ interior mass results in very large ^{46}Ti excesses. The lack of such excesses in the grains indicates that not much material for the outer Si/S and the inner O/Si zones has been in the mixture from which X grains condensed. A similar conclusion has been reached from the lack of large ^{54}Fe excesses in X grains (Marhas et al. 2008). Figures 14(c) and (d) show that some grains have ^{46}Ti

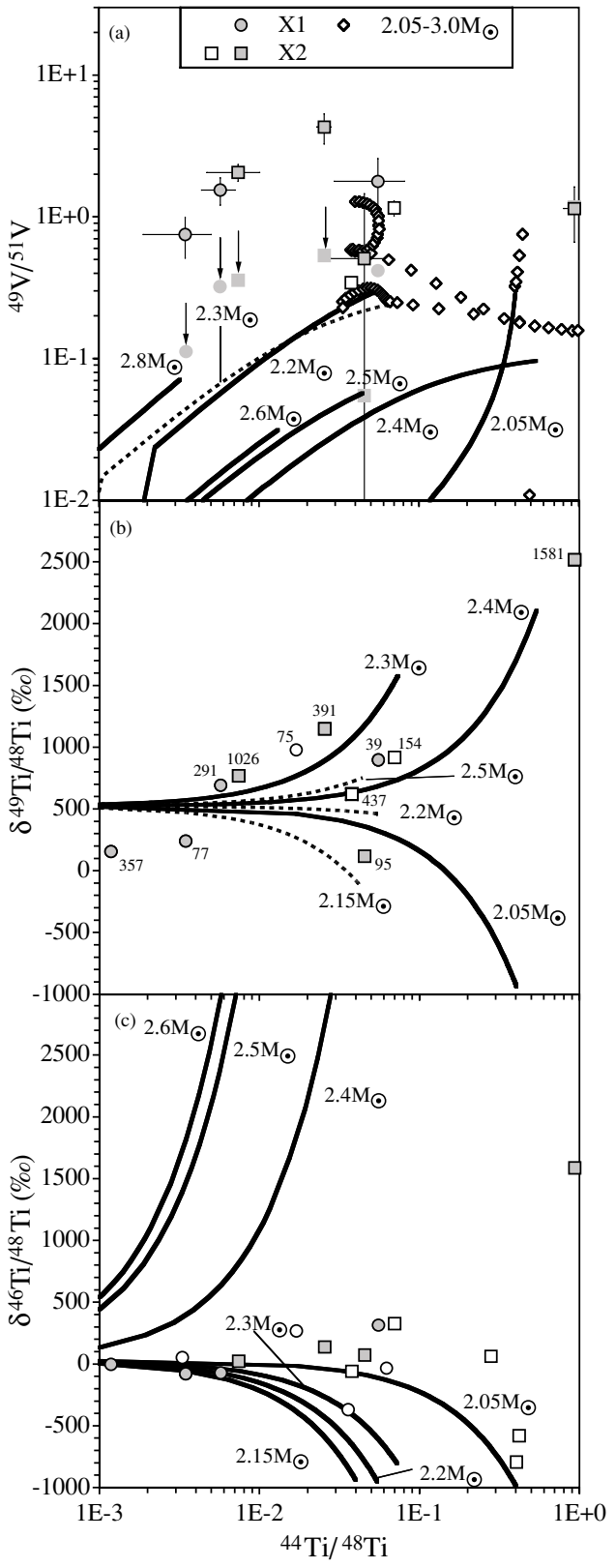

Figure 14. Inferred initial $^{49}V/^{51}V$ ratios and $\delta^{46,49}Ti/^{48}Ti$ values of different subtypes of X grains are plotted as a function of the inferred $^{44}Ti/^{48}Ti$ ratio and compared with theoretical predictions for the 25 $M_\odot$ RAU SN model. The diamonds in panel (a) are the ratios in various layers of the zones containing most of the ^{44}Ti and ^{49}V (see Figure 12(b)). The lines are predictions for the ratios if material from different layers of the Ni, Si/S, and O/Si zones is mixed with a mixture from the He/N and He/C zones. Only mixtures with C/O > 1 are plotted. The numbers next to the data symbols in panel (b) are the $^{12}C/^{13}C$ ratios for these grains. See the text for details.

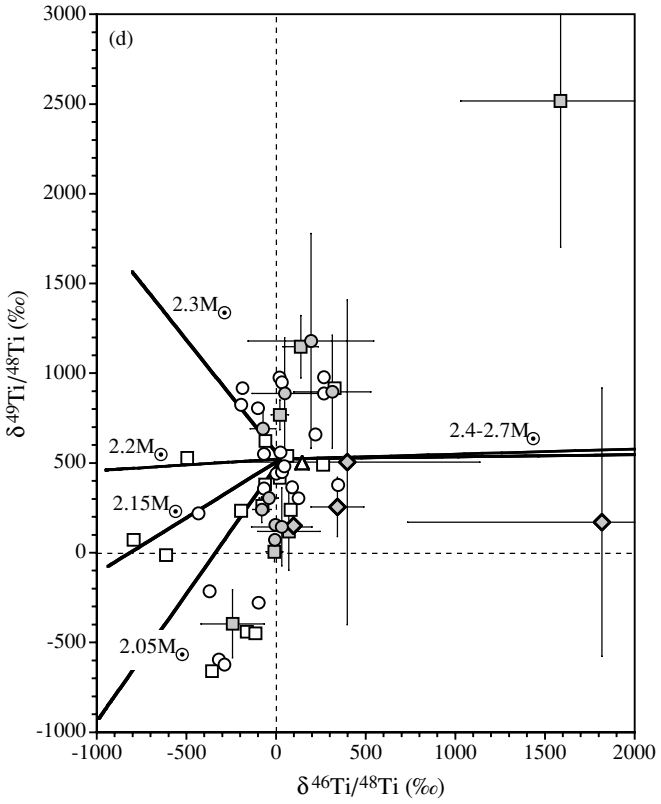

Figure 14. (Continued)

deficits and a few also have ^{49}Ti deficits. These signatures so far have received only scarce attention. Deficits in ^{46}Ti can be explained by admixture of material from the inner Si/S zone (see Figure 12(c)), but ^{49}Ti depletions are more difficult to explain. The layer at 2.05 $M_\odot$ interior mass is very much depleted in ^{49}Ti and its admixture results in negative $\delta^{49}Ti/^{48}Ti$ values (Figure 14(c)). However, as already mentioned, this layer has no ^{28}Si excess and low Si abundance. The layer at 2.15 $M_\odot$ interior mass has ^{28}Si excesses, but its $\delta^{49}Ti/^{48}Ti$ value is only −110‰ and larger ^{49}Ti deficits cannot be explained this way.

4.2. Distinctions Between the Different Subtypes of X Grains

Many isotopic signatures of X grains point to an origin in Type II SNe. However, in order to explain these signatures one has to take material from different zones. In Figure 12, we plot various isotopic ratios and abundances predicted for a 25 $M_\odot$ RAU SN model. Silicon-28 excesses (in the figure shown as $^{29}Si/^{28}Si$ and $^{30}Si/^{28}Si$ ratios smaller than the solar ratios), as well as ^{44}Ti and ^{49}V are found in the Si/S and O/Si zones, high $^{12}C/^{13}C$ and low $^{14}N/^{15}N$ ratios relative to solar in the He/C zone (which also is C-rich, i.e., C/O > 1), and high $^{26}Al/^{27}Al$ ratios in the He/N zone (part of which is also C-rich). We also plot the C/O ratio because equilibrium condensation of SiC requires a C-rich gas where C > O (Lodders & Fegley 1995, 1997). Yoshida & Hashimoto (2004) have tried to reproduce the isotopic ratios of individual X grains through multizone mixing models. We shall not attempt to do so but compare the distributions of selected isotopic ratios and correlations between them with theoretical SN models, similar to the approach used by Travaglio et al. (1999), somewhat analogous to population synthesis in astronomy. We shall not even consider all isotopic data but concentrate on those that show differences for the different subtypes of X grains.

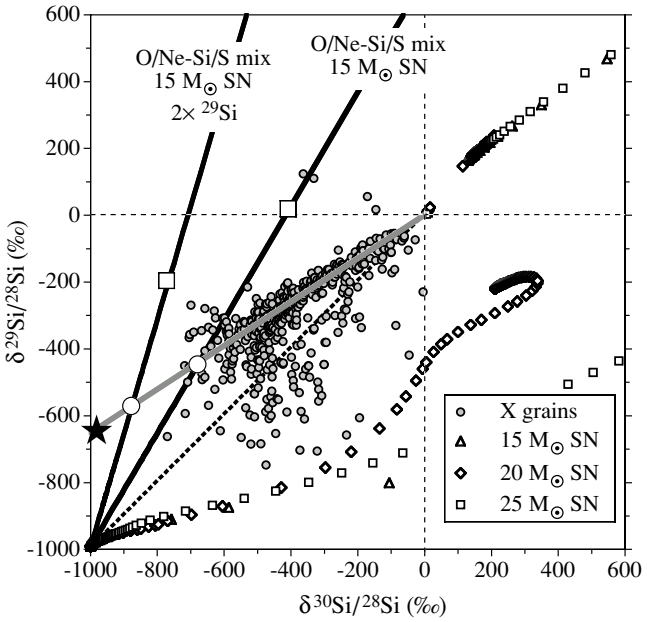

Figure 15. Silicon isotopic ratios of SiC X grains are plotted together with predictions from the 15, 20, and 25 $M_\odot$ SN models by RAU. The oblique gray solid line is the correlation line for X1 grains, the oblique broken line a mixing line between Si of solar isotopic composition with pure ^{28}Si. The star indicates a hypothetical isotopic composition whose mixing with solar Si would explain the isotopic ratios of X1 grains. The two black solid lines are mixing lines between material from the O/Ne zone at 2.5 $M_\odot$ interior mass and the Si/S zone at 1.87 $M_\odot$ interior mass for the 15 $M_\odot$ Rauscher model. For one line, the ^{29}Si yield in the O/Ne zone has been increased by a factor of 2 (Hoppe et al. 2009). The large open circles indicate Si isotopic compositions that, if mixed with normal Si, would reproduce the trend of the X1 grains. The large open squares are compositions obtained if the mixing ratio between Si/S and O/Ne material is only half of that for the open circles.

4.2.1. Silicon, C, N, and Al Isotopes

We start with a comparison of the Si isotopic compositions of X grains with the predictions of the SN models for three different masses of RAU in Figure 15. The figure shows only the region of the grain data; there are some very ^{29}Si- and ^{30}Si-rich compositions in the O/Ne and O/C zones (see Figure 12(b)) that plot outside of the displayed region. It is obvious from Figure 15 that the Si isotopic ratios of most X grains, in particular X1 grains, cannot be reproduced by the SN models. Mixing between material of isotopically normal Si with ^{28}Si-rich material from the Si/S and O/Si zones can reproduce the compositions of only those grains that plot on or below the broken line. This line is a mixing line between pure ^{28}Si ($\delta^{29,30}$Si/^{28}Si = −1000‰) and isotopically normal Si ($\delta^{29,30}$Si/^{28}Si = 0). To explain the ratios of most of the X1 grains requires a component with a composition close to the star in Figure 15. This would be a component with a ^{29}Si/^{28}Si ratio of ∼0.024 (the solar ratio is 0.051) and essentially no ^{30}Si. No SN model to date has produced such a composition in a given layer. The existence and abundance of X1 grains indicate that SNe must produce more ^{29}Si than the models can account for. Timmes & Clayton (1996) have pointed out that SN models produce approximately equal amounts of ^{29}Si and ^{30}Si and cannot account for the solar ^{29}Si/^{30}Si ratio of 1.51. While the solar ratio is the result of contributions from many stellar sources, the remarkable correlation of the Si ratios in X1 grains imposes a fairly tight constraint: it means that the proposed hypothetical component (the star in Figure 15) must be well represented in different SNe.

So far we have considered only binary mixing. Hoppe et al. (2009) reported a SiC grain with a large ^{29}Si excess (δ^{29}Si/^{28}Si = 634‰) and ^{30}Si deficit (δ^{30}Si/^{28}Si = −177‰). The authors explain these isotopic ratios by taking the 15 $M_\odot$ RAU SN model and assuming that the ^{29}Si yield in the O/Ne and O/Si zones is twice that of the model because of a proposed increase in the ^{26}Mg(α,n)^{29}Si reaction rate. In the 15 $M_\odot$ SN model the solar-normalized excess of ^{29}Si over ^{30}Si is more pronounced than in the 25 $M_\odot$ SN model (Figure 12(b)). Doubling the ^{29}Si yield gives a Si isotopic composition that plots in the right upper quadrant of Figure 15 but outside of the limits of the figure, with a much higher δ^{29}Si/^{28}Si than δ^{30}Si/^{28}Si value. Mixing of this material with essentially pure ^{28}Si can reproduce the Si isotopic ratios of that particular grain. However, such a scenario cannot reproduce the correlated array of the X1 grains. In a three-isotope plot such as in Figure 15, any isotopic composition can be obtained by mixing of three components as long as the composition in question lies within the triangle spanned by the three components. Thus, in principle, the isotopic ratios of the X1 grains can be reproduced by mixing of essentially pure ^{28}Si from the Si/S zone, the ^{29}Si-rich component from the O/Ne zone of a 15 $M_\odot$ SN model considered by Hoppe et al. (2009), and a component from the O/C zone where δ^{30}Si/^{28}Si > δ^{29}Si/^{28}Si (see Figure 12(a)).

The question is why such a mix would produce the tight trend shown by the X1 grains and not a wide distribution of ratios. To demonstrate that in Figure 15 we show two mixing curves between material from the 2.5 $M_\odot$ interior mass layer of the O/Ne zone from the 15 $M_\odot$ RAU SN model and the Si/S zone, one with a twofold increase in the ^{29}Si yield in the O/Ne zone and the other without it. The large open circles in the figure indicate compositions that, when mixed with isotopically normal Si would reproduce the correlation line for the X1 grains. However, it is not clear what is so magic about these particular mixing ratios between the O/Ne and Si/S zones. For example, if we add only half as much Si/S material to O/Ne material, we obtain Si isotopic ratios depicted by the large open squares in Figure 15. In this case, we would completely miss the X1 grain compositions. Another consideration that makes such an explanation for the X1 trend unlikely is the following. The O/Si layer lying between the Si/S and O/Ne zones has a large ^{30}Si excess relative to the ^{29}Si excess (see Figure 3 of Hoppe et al. 2009). In addition, the Si abundance of the O/Si zone is at least an order of magnitude higher than that of the O/Ne zone. Contributions from this zone would shift the O/Ne compositions in Figure 15 to compositions with higher ^{30}Si/^{29}Si ratios, i.e., to the right in the plot. In summary, while, yes, the Si isotopic ratios of the X1 grains can be obtained by mixing of three components, it requires a lot of ad hoc fine tuning to reproduce the trend shown by the X1 grains. We consider such an explanation as extremely unlikely and unsatisfactory and are still hoping that future SN models will produce a primary composition close to the star or the open circles in Figure 15.

In order to circumvent the problem of mixing between distant SN zones, Deneault et al. (2003) proposed formation of SiC X grains in a SN region where the Si abundance is at least 10 times the C abundance. In the 25 $M_\odot$ SN model they considered the region between 2.7 and 3.2 $M_\odot$ interior mass. One problem with this proposal is that this region is extremely rich in oxygen (O/C ratios are >100; see Figure 12(a)). Ebel & Grossman (2001) have raised doubts that SiC can condense from a gas with O > C even if C and O are not bound into CO, an assumption made by Deneault et al. (2003). In addition, the predicted isotopic ratios of SiC formed in this region do not agree with those measured in the grains. The predicted Si

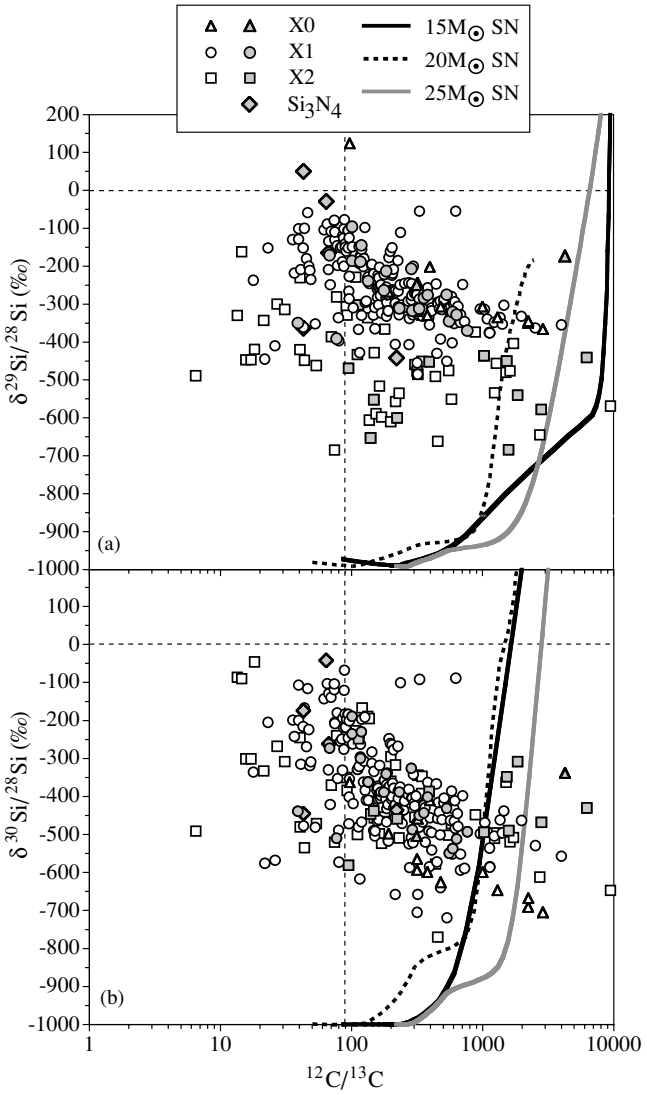

Figure 16. Silicon isotopic ratios of X grains are plotted vs. their $^{12}C/^{13}C$ ratios. Also plotted are the ratios predicted for the Si/S and O/Si zones of the 15, 20, and 25 $M_\odot$ SN models by RAU.

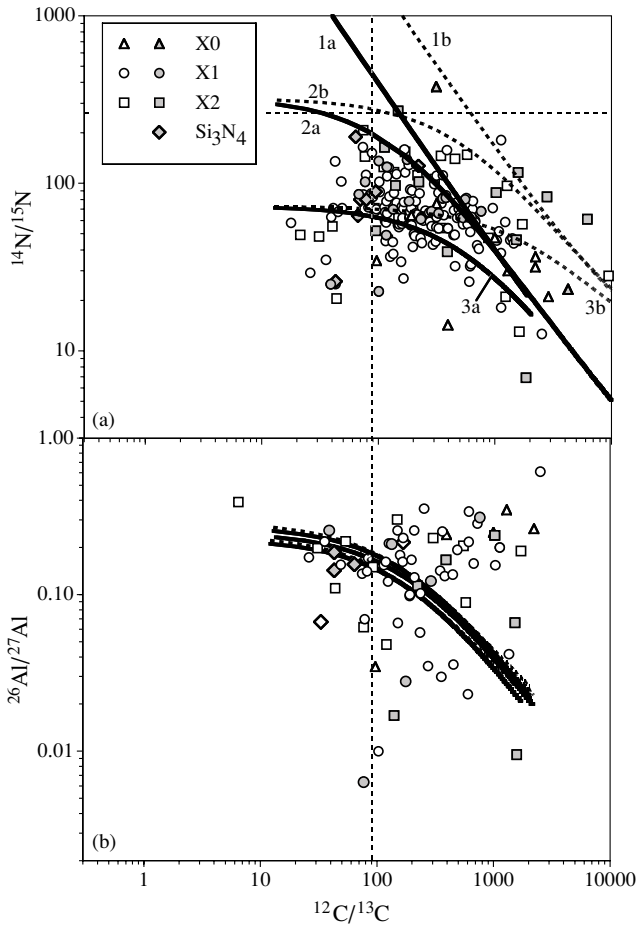

Figure 17. $^{14}N/^{15}N$ (panel (a)) and inferred initial $^{26}Al/^{27}Al$ (panel (b)) ratios of X grains are plotted against their $^{12}C/^{13}C$ ratios. The lines are predicted isotopic ratios obtained by mixing two layers form the He/C zones (Mix a and b) with three layers (Mix 1, 2, and 3) of the He/N zones of the 25 $M_\odot$ SN model by RAU. See the text for details.

isotopic ratios (those in Figure 15 without any mixing with normal Si) are now missing those of all the grains, even those of the X2 grains. The situation is even worse if we consider the Si and C isotopic compositions together. Figure 16 shows plots of the Si versus the C isotopic ratios of X grains. There is a certain correlation between those ratios in the sense that there is a cutoff above which only very few grains plot. Nittler & Alexander (2003) have noticed such a cutoff for $\delta^{29}Si/^{28}Si$ and $^{12}C/^{13}C$ also for mainstream, Y, and Z grains, believed to come from AGB stars and that this cutoff extends to lower $^{12}C/^{13}C$ and higher $\delta^{29}Si/^{28}Si$ values. Figure 16(a) shows that most X2 grains plot below the X1 grains, i.e., have smaller $^{29}Si/^{28}Si$ ratios, as is clear from the Si three-isotope plot (Figure 2). The fraction of grains with $^{12}C/^{13}C > 1000$ depends on subtype. It is 33%, 5.4%, and 20% for X0, X1, and X2 grains, respectively. This is also reflected in the averages for the $^{12}C/^{13}C$ ratio, which are 1113, 304, and 665 for the three subtypes. In Figure 16, we also plot the C and Si isotopic ratios in the Si/S and O/Si zones of three RAU SN models. The predicted ratios miss most of the grains and instead of the overall negative slope of the correlations shown by the grains, the theoretical curves have positive slopes. The situation is also untenable concerning the N isotopic ratios in the Si/S and O/Si zones. In Figure 12(a), it can be seen that the $^{14}N/^{15}N$ ratio is at least a factor of 1000 below solar, i.e., smaller than 0.3. However, almost all X grains have $^{14}N/^{15}N$ ratios between 10 and 100 (Figure 17(a)).

We conclude that we have to mix material from the Si/S zone to material from the He/C and He/N zones (and possibly the H zone) in order to even approximately reproduce the isotopic signatures of the X grains and to achieve C > O. We say approximately, because all observed correlations cannot be reproduced in detail. We have already pointed out that the Si isotopic ratios of the X1 grains cannot be explained by existing SN models without making unlikely ad hoc mixing assumptions, because no model produces a primary composition close to the star symbol in Figure 15. In order to reproduce the range of $^{12}C/^{13}C$ ratios observed in X grains, mixing between the He/C and He/N zones is required. In the first of these zones, He burning produces ^{12}C, resulting in very high $^{12}C/^{13}C$ ratios, and in the second, H burning in the CNO cycle results in a $^{12}C/^{13}C$ ratio of ∼3.5. Figure 17 shows the grains' C, N, and Al isotopic data and ratios produced if we add He/C-zone material to He/N-zone material with variable mixing ratios in the 25 $M_\odot$ RAU SN model. Mixes labeled **a** take material from the He/C layer at 7.24 $M_\odot$ interior mass, just outside of the boundary with the O/C zone (see Figure 12(b)); mixes labeled **b** take material from 7.6 $M_\odot$ interior mass. The first layer has a large

^{15}N excess, i.e., a low ^{14}N/^{15}N ratio, and large ^{29}Si, ^{30}Si, and ^{49}Ti excesses, but in the second layer, these excesses are more moderate (see Figure 12(b); the Ti isotopic ratios are not shown there). In the He/N zone, we chose three different layers: the first is at 8.2 $M_\odot$ interior mass, the second from the ^{15}N-rich spike at 8.33 $M_\odot$ interior mass, the third the average of 20% of the He/N zone centered on the layer at 8.33 $M_\odot$ interior mass.

As can be seen in Figure 17(a), mixing of these combinations covers most of the C and N grain data fairly well. The He/C zone is ^{12}C- and ^{15}N-rich, with ^{14}N/^{15}N ratios decreasing as one traverses the zone from the outer to the inner boundary (Figure 12(b)). Thus, admixture of He/C material increases the ^{12}C/^{13}C ratio and decreases the ^{14}N/^{15}N ratio (Figure 17(a)). The N–C diagram shows that the sense of the correlation (a negative slope) shown by the grain data is reproduced by the mixing model, but reveals already some of the problems. In order to cover the isotopic ratios of most grains, we have to start with a low ^{14}N/^{15}N ratio in the He/N zone as represented by the ^{15}N-rich spike. However, if we take the average of 20% of the zone centered on this spike (Mix 3), we miss most of the data points, even more so if we would take the average of the whole He/N zone. In addition, we have to admix material from a layer at the bottom of the He/C zone (Mix a), otherwise we also miss most of the data points. In other words, we have to make very special, ad hoc, assumptions in order to reproduce the C–N data. An additional puzzle is that the ^{15}N-rich spike in the He/N zone that shows up in the RAU 25 $M_\odot$ SN model does not appear in their 15 $M_\odot$ and 20 $M_\odot$ models, nor in any of the Woosley & Weaver (1995) SN models and the models by Limongi and Chieffi (2003; 2009). As a matter of fact, the 15 $M_\odot$ and 20 $M_\odot$ models by the latter authors do not produce any ^{15}N excesses in the He/C zone, and in more interior zones the N abundances are so low that they cannot affect the N isotopic compositions of the grains. We defer a more detailed study of this problem to the future.

In the C–N plot (Figure 17(a)), X2 grains with ^{12}C/^{13}C ratios above 300 have, on average, higher ^{14}N/^{15}N ratios than X0 and X1 grains. This is a puzzle, because the C and N isotopic ratios of the grains are dominated by contributions from the outer zones whereas the Si isotopic compositions need contributions from the Si/S and O/Si zones to explain the ^{28}Si excesses in X grains. However, these inner zones have negligible contents of C and N. It is not clear why C–N and Si isotopic ratios should be correlated. Considering different mass models does not help us as long as none of the existing models can explain the Si isotopic ratios of most of the X grains (specifically the X1 grains) in a satisfactory fashion.

There are more problems with the He/N–He/C mixing models. Figure 17(b) shows the results of the mixing for the ^{26}Al/^{27}Al and ^{12}C/^{13}C ratios. Because ^{26}Al/^{27}Al ratios are very similar in the He/N layers selected for our mixing exercise and much lower in the He/C zone (see Figure 12(b)), the different mixing curves are very close to one another. Unfortunately, they not only miss most of the data points, the general trend in the grain data, i.e., increasing ^{26}Al/^{27}Al ratios with increasing ^{12}C/^{13}C ratios, is not reflected in the negative slope of the mixing models. Small inferred ^{26}Al/^{27}Al ratios might be the result of contamination with Al from adjacent Al-rich grains during the ion probe analysis, but the high ^{26}Al/^{27}Al ratios combined with high ^{12}C/^{13}C ratios shown by many grains clearly disagree with the mixing models. The ^{26}Al/^{27}Al ratio in the outer He/N zone decreases toward the H-rich envelope (Figure 12(a)), thus a component from this part or the average over the whole He/N zone would have resulted in lower mixing curves in Figure 17(b). In all existing SN models, the He/N zone is the only place where the predicted ^{26}Al/^{27}Al ratio approaches the ratios observed in X grains and where there is enough Al to affect the compositions of the grains. In all other zones, except the inner Ni zone (at 2.05 $M_\odot$ inner mass in the 25 $M_\odot$ RAU SN model), this ratio is much smaller (Figure 12(b)). However, as mentioned previously, this layer does have larger-than-solar ^{29,30}Si/^{28}Si ratios and the Al concentration is too low to make any significant contribution to the grains. As a result of H burning in the CNO cycle, the ^{12}C/^{13}C in the He/N zone is very low (3.5). In order to obtain the high ^{12}C/^{13}C ratios observed in the grains, one has to admix material from the He/C zone, in the process lowering the ^{26}Al/^{27}Al ratio. This is a long-recognized problem. In addition, for Mix 1a that gives ^{12}C/^{13}C = 390 and ^{14}N/^{15}N = 100 we obtain δ^{49}Ti/^{48}Ti = 6375‰, a value much higher than any that has been measured in an X grain (see Figure 7). For this case the C/O ratio is 17 and the C/Si ratio is 30. Such a high ratio would favor the condensation of graphite over SiC (Lodders & Fegley 1997). The bottom of the He/C zone is enriched in ^{29}Si and ^{30}Si (see Figure 12(b)) and Mix 1a with the above C and N isotopic ratios has δ^{29}Si/^{28}Si = 800‰ and δ^{30}Si/^{28}Si = 1,100‰.

Figure 18 shows the Si isotopic ratios resulting from mixing the above described Mix 1a (^{12}C/^{13}C = 390) with different layers from the Si/S and O/Si zones (see Figure 12(a)). All the compositions obtained from mixing with layers from 2.3 $M_\odot$ to 2.7 $M_\odot$ interior mass lie on lines between the Mix 1a composition of δ^{29}Si/^{28}Si = 800‰ and δ^{30}Si/^{28}Si = 1100‰ and the origin (pure ^{28}Si). Since the O abundance of the layers in these zones increases as we move outward, the O/C ratio becomes greater than unity at some mixing ratio. In Figure 18, we indicated the Si isotopic compositions where this is the case for mixing with layers at 2.5, 2.6, and 2.7 $M_\odot$ interior mass. Only at the 2.8 $M_\odot$ layer is the Si isotopic composition sufficiently ^{30}Si-rich (see Figure 12(a)) that we move substantially away from the other mixing lines. While mixing with the Si/S and O/Si layers produces the whole range in the ^{29}Si/^{28}Si and ^{30}Si/^{28}Si ratios observed in X grains (although not with the correct relative relationship between them), the C isotopic ratio of the original He/N–He/C mix remains essentially constant. The reason is that the Si/S and O/Si zones contain so little C that admixture from these zones does not affect the C isotopic ratios. In Si versus C isotopic ratio plots such as those in Figure 16, these mixing lines would be vertical lines for different ^{12}C/^{13}C ratios resulting from the original He/N–He/C mix. In other words, the C and Si isotopic ratios are completely decoupled from one another and mixing cannot explain the general trend observed in the grains (Figure 16).

A possible explanation for this trend and the upper cutoff in the plots of Figure 16 might be the following. As mentioned above, the C/O ratio of the Mix 1a composition considered here is very high, probably inhibiting SiC formation in favor of graphite. As material from the Si/S or O/Si zone is admixed to this composition, the ^{29,30}Si/^{28}Si ratios decrease whereas the ^{12}C/^{13}C ratio stays constant. However, in the case of admixture from the O/Si zone, O is added and the C/O ratio decreases. At some mixing ratio, the C/O ratio will approach unity, enabling the formation of SiC. This would explain the sharp upper cutoff in Figures 16(a) and (b), i.e., why for a given ^{12}C/^{13}C ratio there are no grains with ^{29,30}Si/^{28}Si ratios above some limiting values. In principle, it also explains the slope of the cutoff. For a higher ^{12}C/^{13}C ratio of the He/N–He/C mix, the C/O ratio will also be higher. This means that more material from the

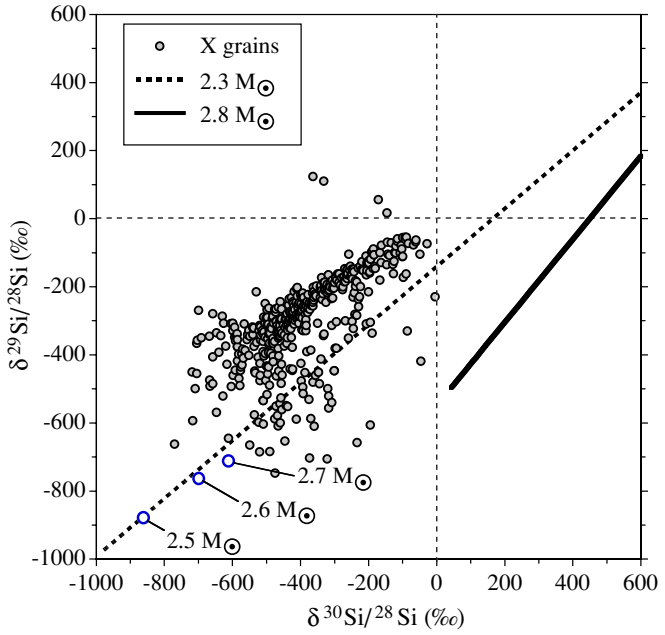

Figure 18. Silicon isotopic ratios of X grains and mixing lines between a mixture of the He/N and He/C zones (see the text) and material from different layers of the Si/S (2.3 $M_\odot$ interior mass) and O/Si zones (2.8 $M_\odot$). Only C-rich (C > O) final compositions are plotted. The open circles are the compositions where C/O = 1. The lines from these points are essentially the same as the 2.3 $M_\odot$ line, only truncated.

(A color version of this figure is available in the online journal.)

O/Si zone has to be admixed in order to lower the C/O ratio to close to unity, resulting in lower $^{29,30}Si/^{28}Si$ ratios. In practice, the situation is complicated. For example, if we mix He/N–He/C Mix 1a considered above ($^{12}C/^{13}C = 390$, $^{14}N/^{15}N = 100$, $\delta^{29}Si/^{28}Si = 800‰$, and $\delta^{30}Si/^{28}Si = 1{,}100‰$) with material from the layer of interior mass 2.5 $M_\odot$, the $\delta^{29}Si/^{28}Si$ and $\delta^{30}Si/^{28}Si$ values reached when C/O = 1 are −885‰ and −864‰, respectively. These values are below essentially all the grain data at $^{12}C/^{13}C = 390$ (Figure 16). If we move farther out in the O/Si zone, the $\delta^{29,30}Si/^{28}Si$ values become larger (−819‰ and −769‰ at interior mass 2.6 $M_\odot$, and −755‰ and −667‰ at interior mass 2.7 $M_\odot$). However, at interior mass 2.8 $M_\odot$, the values are −532‰ and +13‰. This behavior reflects the fact that $\delta^{30}Si/^{28}Si > \delta^{29}Si/^{28}Si$ in the starting Mix 1a and also in the O/Si zone (Figure 12(a)). We can, of course, use different He/N–He/C mixes, giving different initial ^{29}Si and ^{30}Si excesses, but the basic fact that $\delta^{30}Si/^{28}Si$ will be larger than $\delta^{29}Si/^{28}Si$ is not going to change. The same behavior is obtained from the 15 $M_\odot$ and 20 $M_\odot$ models as well, another example that SN models cannot reproduce the grain data in all details. However, there is a fundamental problem with this scenario. As discussed previously in connection with the Ti isotopic ratios of the grains, any contributions from layers between 2.4 $M_\odot$ and 2.8 $M_\odot$ interior are predicted to result in large ^{46}Ti excesses, which are not observed in the grains. Since Ti exists in Ti-rich subgrains (possibly TiC) within X grains (see Figures 9 and 11), these subgrains might have formed before SiC condensation in a different SN region. In this case, the Ti isotopic compositions of the grains would not necessarily have to be related to their Si isotopic compositions and the C/O ratio of the region where the grains formed. It is clear that fractionation between Ti and Si (and other elements) because of independent formation of TiC grains adds another layer of complexity to formation scenarios. We have to defer dealing with this possibility.

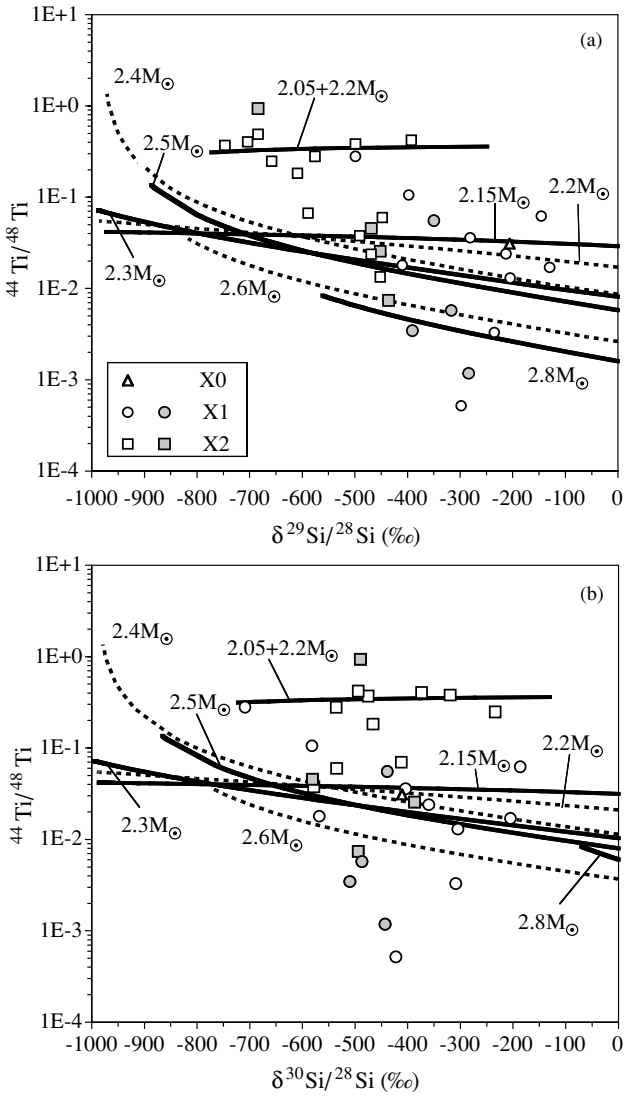

Figure 19. Inferred initial $^{44}Ti/^{48}Ti$ ratios of X grains are plotted against their Si isotopic ratios. The lines are obtained by mixing material from different layers of the Si/S and O/Si zones with a mixture between the He/N and He/C zones; the line labeled 2.05+2.2 $M_\odot$ combines contributions from the inner Ni zone with the Si/S zone (see the text).

4.2.2. Titanium-44 and Si Isotopic Ratios

Besides the Si (Figures 1 and 2) and N (Figure 17) isotopic ratios, the inferred $^{44}Ti/^{48}Ti$ ratios show a clear distinction between Group X1 and X2 grains (Figure 6). $^{44}Ti/^{48}Ti$ ratios are higher in X2 grains than in X1 grains. A correlation between $^{44}Ti/^{48}Ti$ ratios and Si isotopic ratios is expected since the zones containing ^{44}Ti are rich in ^{28}Si (Figure 12(a)). However, such a correlation is observed only for the $^{29}Si/^{28}Si$ ratio (Figure 6(b)) and not for the $^{30}Si/^{28}Si$ ratio (Figure 6(c)). One thing is clear: to account for the initial presence of ^{44}Ti in X grains, we have to mix material from the Si/S and/or O/Si zones with material from other zones needed to explain the C, N, and Al isotopic ratios of the grains.

In Figure 19, we show mixing curves obtained by mixing He/N–He/C Mix 1a (C/O = 16, $^{12}C/^{13}C = 390$, $^{14}N/^{15}N = 100$, $\delta^{29}Si/^{28}Si = 800‰$, and $\delta^{30}Si/^{28}Si = 1{,}100‰$) with material from different layers of the Ni, Si/S, and O/Si zones (see Figure 12(b)). As can be seen from the plots, while the sign of the correlation between the $^{44}Ti/^{48}Ti$ and $^{29}Si/^{28}Si$ ratios is

reproduced by the mixing curves, and while the data for X1 grains can be accounted for by the SN model, most of the X2 grains plot above the curves. Although the ^{44}Ti abundances are highest in the Ni zone (Figure 12(b)), the high ^{48}Ti abundance there results in ^{44}Ti/^{48}Ti ratios that are lower than those in the outer Si/S and inner O/Si zones (Figure 12(c)). The ratio is highest in the layer at 2.4 $M_\odot$, and as a consequence the mixing curve with this layer reaches the highest ^{44}Ti/^{48}Ti ratio (Figure 19). However, the corresponding ^{29,30}Si/^{28}Si ratios are much lower than those measured in the grains. As in previous plots, mixing curves are shown only for mixtures with C > O. This explains why the curves for the 2.5, 2.6, and 2.8 $M_\odot$ layers terminate at increasing $\delta^{29,30}$Si/^{28}Si values.

The layer at 2.05 $M_\odot$ interior mass does not have a ^{28}Si excess and is low in Si (Figure 12(b)) and its admixture does not produce the Si isotopic ratios of the grains. However, if we combine contributions from this layer and layers above that carry ^{28}Si, we can achieve higher ^{44}Ti/^{48}Ti ratios together with the range if Si isotopic ratios seen in X2 grains. For example, the curves labeled "2.05 + 2.2 $M_\odot$" in Figure 19 were obtained with 10% from the 2.05 $M_\odot$, 0.6%–3% from the 2.2 $M_\odot$ layer, and the remaining fraction from our He/N–He/C mix described above. This resulting mixture comes close to reproducing the ratios of most X2 grains, although it does not reach the highest measured ratios (^{44}Ti/^{48}Ti = 0.4 ratio at 2.05 $M_\odot$ interior mass). This confirms the conclusion of Hoppe et al. (1996) that contributions from the Ni core have to be included in order to explain the inferred ^{44}Ti/^{48}Ti of some of the grains.

For the mixing curves with the 2.15 and 2.2 $M_\odot$ layers and the 2.05+2.2 $M_\odot$ mixing curve, the high resulting C/O ratio, which essentially remains the same (16) as that of the He/N–He/C mix, might be a problem because it is not clear whether SiC can condense from a gas with such a high C/O ratio. However, we note that the Si/C ratios in the mixed material are fairly high, higher than the O/C ratio. For example, in the mix with the 2.05+2.2 $M_\odot$ layers, the Si/C ratio is 0.23 at δ^{29}Si/^{28}Si = −750‰. However, the Fe/Si and Fe/C ratios for this mix are 14 and 3.8, respectively. It remains to be seen whether SiC can condense under such conditions. A possibility is that the C-rich mix from the outer layers contains also some material from the O/C zone. The C content of this zone is high (actually much higher than that of the He/C zone; it is just that the O content is even higher) and the ^{12}C/^{13}C ratio is also extremely high (see Figure 12(a)). A proper mix might result in a moderate C/O ratio. A smaller C/O ratio would also help with the problem we had in reproducing the upper cutoff in the $\delta^{29,30}$Si/^{28}Si versus ^{12}C/^{13}C ratio plots (Figure 16). With the high C/O ratios of our He/N–He/C mix, we ended up with much too low $\delta^{29,30}$Si/^{28}Si values at C = O when we added material from the lower O/Si zone. If the material with a high ^{12}C/^{13}C ratio from the outer layers including the O/C zone has a smaller C/O ratio, we have to add less material from the O/Si zone and C = O is achieved at higher $\delta^{29,30}$Si/^{28}Si values. However, the high Fe content, a consequence of admixture of Ni core material, might remain a problem. We want to emphasize that the composition of the gas from which X grains condensed is very different from a gas of close-to-solar compositions for which most condensation calculations are performed. The detailed exploration of all multizone mixing possibilities and that of grain condensation from the resulting gas is an extremely complicated problem, exceeding by far the scope of this paper.

5. REMARKS ON SUPERNOVA MODELS

In this paper, we have heavily relied on the SN models by Rauscher et al. (2002), concentrating on the 25 $M_\odot$ model. Among the three models used (15, 20, and 25 $M_\odot$), this model is the only one with a ^{15}N spike in the He/N zone, which is needed to reproduce the C and N isotopic ratios of the grains. For all the other isotopic ratios investigated here, the three SN models lead to essentially the same basic conclusions. Rauscher et al. calculated also a series of models, most of which are listed on the web but not referred to in publications, with varying assumptions about the energy of the explosion, the amount of ^{56}Ni in the core, and some reaction rates, mainly that of the ^{22}Ne(α,n)^{25}Mg reaction. We have not looked at the models in detail but used only the "best" models preferred by the authors.

We did look, however, at the 15, 20, and 25 $M_\odot$ models by Limongi & Chieffi (2003, 2009, hereafter L+C), graciously provided by these authors. These models seem to make it even more difficult to account for some of the grain data than the RAU models. We have already mentioned that the 15 and 20 $M_\odot$ L + C models do not have any ^{15}N excesses in the He/C zone. The 25 $M_\odot$ model does not have a ^{15}N-rich spike in the He/N zone and the ^{15}N abundance is constant throughout the He/C zone. All these features make it more difficult to explain the ^{15}N excesses in the X grains. Another difference is that in the L+C models ^{26}Al/^{27}Al ratios in the He/N zone are smaller than in the RAU models, missing the high ratios in grains even more than the RAU models. In contrast to the RAU models, the L+C models have C/O zones and admixture from these zones can explain the high ^{12}C/^{13}C ratios of most X grains. However, the C/O zones have high ^{14}N/^{15}N ratios and thus would not help with low ^{14}N/^{15}N ratios found in the grains (Figure 17). The Si/S and O/Si zones in the L + C models are narrower than in the RAU models and it might be more difficult to add the required amount of material. In most other aspects, the L + C are similar enough to the RAU models that we do not expect any fundamentally different conclusions.

We followed the suggestion of Hoppe et al. (2009) in increasing the ^{29}Si yield from the O/Ne zone of the 15 $M_\odot$ RAU model. While it is clear that ^{29}Si production in SNe have to be increased beyond what is predicted by models in order to produce the solar Si isotopic ratios (Timmes & Clayton 1996; Lugaro et al. 1999; Travaglio et al. 1999), we concluded that admixture from the O/Ne zone does not provide a satisfactory solution to the problem of the Si isotopic ratios of the X1 grains. However, in future efforts we might consider the grain data as a guide in exploring the consequences of alterations in various reaction rates and assumptions about convection in SN models with the goal to better reconcile theoretical predictions and laboratory data.

6. CONCLUSIONS

We performed isotopic measurements of C, N, Si, Al–Mg, Ca and Ti in SiC and Si_3N_4 grains of type X from the enstatite chondrite Qingzhen. X grains are believed to have formed in the ejecta of Type II SNe. The Si isotopic ratios of X grains indicate the presence of at least two subtypes, X1 and X2 (Lin et al. 2002). Mg, Ca, and Ti isotopic measurements were made to determine initial abundances of the short-lived radioisotopes ^{26}Al, ^{44}Ti, and ^{49}V. The ultimate objective of this study was to see whether differences between X1 and X2 grains are also shown in other isotopic systems besides Si. We compared the isotopic compositions of the grains of this study and of previous

studies by other investigators with theoretical model predictions for Type II SNe by RAU.

From the grain data and the SN models we arrive at the following conclusions.

1. No existing SN models can explain the Si isotopic compositions of most X grains, especially the X1 grains, without invoking very special, highly unlikely mixing conditions, which we find ad hoc and extremely unsatisfactory. To do so in a simple way, the models would have to produce a primary component in which ^{28}Si is accompanied by ^{29}Si with a ratio $^{29}Si/^{28}Si \sim 0.024$ and this component must be ubiquitous among different SNe.
2. The C and N isotopic ratios of X grains contradict the model by Deneault et al. (2003), which proposes that these grains condense directly from layers in the lower O/Si zone, invalidating this model. Material from the He/N and He/C zone is needed to explain the C, N, and Al isotopic ratios of the grains.
3. However, the He/N–He/C mix fails to reproduce the grain data in detail. The N and C isotopic data can be fairly well matched as long as the ^{15}N spike in the He/N zone predicted for the $25\,M_{\odot}$ SN model by RAU is included in some of the mixes. This issue needs further exploration. The fact that X2 grains have higher N isotopic ratios than X1 grains remains unexplained. The SN models fail to account for the inferred $^{26}Al/^{27}Al$ ratios in connection with the $^{12}C/^{13}C$ ratios of the grains. Because the He/N zone has low $^{12}C/^{13}C$ and high $^{26}Al/^{27}Al$ ratios, whereas the He/C zone has high $^{12}C/^{13}C$ and low $^{26}Al/^{27}Al$ ratios, mixing produces a negative correlation between these two ratios, which is not shown by the grain data.
4. The ^{49}Ti excesses found in X grains can be explained as the result of the decay of short-lived ^{49}V only in some grains. In other grains, they must be due to contributions from the He/C zone where ^{49}Ti excesses are produced by neutron capture. The lack of large ^{46}Ti excesses indicates that only limited amounts from the outer Si/S and inner O/Si contributed to the mix from which X grains formed.
5. Inferred $^{44}Ti/^{48}Ti$ ratios are highest in X2 grains and can be reproduced by SN mixing models only if substantial contributions from the inner Ni core are taken into account. These contributions result in high Fe abundances and it is still not clear whether SiC can condense from this type of mixture. The ratios seen in the rest of the grains can be reproduced by mixing with material from the Si/S and the inner region of the O/Si zone.

In summary, as remarked by others before, SN models fail to account in detail for many of the isotopic compositions of X grains. The most glaring problems are the Si isotopic compositions themselves, the fact that most grains, the X1 grains, need a primary component with ^{29}Si, and the high $^{26}Al/^{27}Al$ ratios in grains with high $^{12}C/^{13}C$ ratios (and low $^{14}N/^{15}N$ ratios). We can only hope that the grain data will guide stellar modelers to look for ways to overcome these problems with the models. There are other issues that need to be explored. One is to find out what range of elemental compositions under the temperature and pressure conditions of SN ejecta will allow the condensation of SiC.

This work is supported by the knowledge innovation program of Chinese Academy of Sciences (kzcx2-yw-110), the Natural Science Foundation of China (40830421) and NASA (NNX08AG71G). We thank Alessandro Chieffi, Alexander Heger, and Marco Limongi for providing SN models. We gratefully acknowledge constructive reviews by Peter Hoppe and an anonymous reviewer.

REFERENCES

Amari, S., Hoppe, P., Zinner, E., & Lewis, R. S. 1992, ApJ, 394, L43
Amari, S., Hoppe, P., Zinner, E., & Lewis, R. S. 1995, Meteoritics, 30, 679
Bernatowicz, T. J., Amari, S., & Lewis, R. S. 1992, Lunar Planet. Sci., XXIII, 91
Besmehn, A. 2001, PhD thesis, Johannes-Gutenberg-Universität, Mainz
Besmehn, A., & Hoppe, P. 2003, Geochim. Cosmochim. Acta, 67, 4693
Clayton, D. D., & Nittler, L. R. 2004, Annu. Rev. Astron. Astrophys., 42, 39
Deneault, E. A.-N., Clayton, D. D., & Heger, A. 2003, ApJ, 594, 312
Ebel, D. S., & Grossman, L. 2001, Geochim. Cosmochim. Acta, 65, 469
Gyngard, F., Amari, S., Jadhav, M., Marhas, K., Zinner, E., & Lewis, R. S. 2006, Meteorit. Planet. Sci., 41, A71
Henkel, T., Stephan, T., Jessberger, E. K., Hoppe, P., Strebel, R., Amari, S., & Lewis, R. S. 2007, Meteorit. Planet. Sci., 42, 1121
Hinton, R. W. 1990, Chem. Geol., 83, 11
Hoppe, P. 2004, in ASP Conf. Ser. 309, Astrophysics of Dust, ed. A. Witt, G. C. Clayton, & B. T. Draine (San Francisco, CA: ASP), 265
Hoppe, P., Amari, S., Zinner, E., Ireland, T., & Lewis, R. S. 1994, ApJ, 430, 870
Hoppe, P., & Besmehn, A. 2002, ApJ, 576, L69
Hoppe, P., Leitner, J., Meyer, B. S., The, L.-S., Lugaro, M., & Amari, S. 2009, ApJ, 691, L20
Hoppe, P., Strebel, R., Eberhardt, P., Amari, S., & Lewis, R. S. 1996, Science, 272, 1314
Hoppe, P., Strebel, R., Eberhardt, P., Amari, S., & Lewis, R. S. 2000, Meteorit. Planet. Sci., 35, 1157
Huss, G. R., Hutcheon, I. D., & Wasserburg, G. J. 1997, Geochim. Cosmochim. Acta, 61, 5117
Hynes, K. M., Croat, T. K., Amari, S., Mertz, A. F., & Bernatowicz, T. J. 2006, Meteorit. Planet. Sci., 41, A83
Kane, J. S. 1998, Geostand. Newsl.: J. Geostand. Geoanal., 22, 7
Limongi, M., & Chieffi, A. 2003, ApJ, 592, 404
Limongi, M., & Chieffi, A. 2009, ApJ, 647, 483
Lin, Y., Amari, S., & Pravdivtseva, O. 2002, ApJ, 575, 257
Lodders, K., & Amari, S. 2005, Chem. Erde Geochem., 65, 93
Lodders, K., & Fegley, B., Jr. 1995, Meteoritics, 30, 661
Lodders, K., & Fegley, B., Jr. 1997, in AIP Conf. Proc. 402, Astrophysical Implications of the Laboratory Study of Presolar Materials, ed. T. J. Bernatowicz & E. Zinner (Melville, NY: AIP), 391
Lodders, K., & Fegley, B., Jr. 1999, in IAU Symp. 191, Asymptotic Giant Branch Stars, ed. T. Le Bertre, A. Lèbre, & C. Waelkens (San Francisco, CA: ASP), 279
Lugaro, M. 2005, Stardust from Meteorites (Singapore: World Scientific)
Lugaro, M., Zinner, E., Gallino, R., & Amari, S. 1999, ApJ, 527, 369
Marhas, K. K., Amari, S., Gyngard, F., Zinner, E., & Gallino, R. 2008, ApJ, 689, 622
Nittler, L. R. 1996, PhD thesis, Washington University, St. Louis
Nittler, L. R., & Alexander, C. M. O'D. 2003, Geochim. Cosmochim. Acta, 67, 4961
Nittler, L. R., Alexander, C. M. O'D., Gao, X., Walker, R. M., & Zinner, E. 1997, ApJ, 483, 475
Nittler, L. R., Amari, S., Zinner, E., Woosley, S. E., & Lewis, R. S. 1996, ApJ, 462, L31
Nittler, L. R., & Hoppe, P. 2005, ApJ, 631, L89
Nittler, L. R., et al. 1995, ApJ, 453, L25
Rauscher, T., Heger, A., Hoffman, R. D., & Woosley, S. E. 2002, ApJ, 576, 323 (RAU)
Rocholl, A. B. E., et al. 1997, Geostand. Newsl.: J. Geostand. Geoanal., 21, 101
Timmes, F. X., & Clayton, D. D. 1996, ApJ, 472, 723
Timmes, F. X., Woosley, S. E., Hartmann, D. H., & Hoffman, R. D. 1996, ApJ, 464, 332
Travaglio, C., Gallino, R., Amari, S., Zinner, E., Woosley, S., & Lewis, R. S. 1999, ApJ, 510, 325
Woosley, S. E., & Weaver, T. A. 1995, ApJS, 101, 181
Yoshida, T., & Hashimoto, M. 2004, ApJ, 606, 592
Zinner, E. 2007, in Treatise on Geochemistry Update, ed. H. D. Holland, K. K. Turekian, & A. Davis (Oxford: Elsevier), 1, 1.02 (online update only)
Zinner, E., Amari, S., Anders, E., & Lewis, R. S. 1991, Nature, 349, 51
Zinner, E., et al. 2007, Geochem. Cosmochim. Acta, 71, 4786